

# Nonlinear dynamics of matrix-cracked hybrid laminated plates containing carbon nanotube-reinforced composite layers resting on elastic foundations

Yin Fan · Hai Wang

Received: 30 March 2015 / Accepted: 13 December 2015 / Published online: 23 December 2015  
© Springer Science+Business Media Dordrecht 2015

**Abstract** This paper investigates the nonlinear dynamic response of hybrid laminated plates resting on elastic foundations in thermal environments. The plate consists of conventional fiber-reinforced composite (FRC) layers and carbon nanotube-reinforced composite (CNTRC) layers. Each layer may have matrix cracks, and the damage is described by a refined self-consistent model. The motion equations are based on a higher-order shear deformation theory with a von Kármán type of kinematic nonlinearity. The thermal effects are included, and the material properties of both FRC and CNTRC are assumed to be temperature dependent. The plate–foundation interaction is also included. The motion equations are solved by a two-step perturbation technique to determine the dynamic response of matrix-cracked hybrid laminated plates. The boundary condition is assumed to be simply supported with in-plane displacements “movable” or “immovable.” The effects of stiffness reduction due to matrix cracks, the foundation stiffness, the temperature change, the percentage and distribution of carbon nanotubes in CNTRC layers are discussed in detail through a parametric study.

**Keywords** Nonlinear dynamics · Hybrid laminated plate · Matrix crack · Elastic foundation · Temperature-dependent properties

---

Y. Fan · H. Wang (✉)  
School of Aeronautics and Astronautics, Shanghai Jiao  
Tong University, Shanghai 200240,  
People’s Republic of China  
e-mail: wanghai601@sjtu.edu.cn

## 1 Introduction

As is well known, fiber-reinforced composite (FRC) materials have been widely used in aerospace industry due to its outstanding properties. However, cracks in a structural element cause local stiffness reduction [1] and change the global static and dynamic characteristics [2]. Hence, it is of prime importance to understand the vibration characteristics of cracked structures in structural health monitoring and nondestructive damage evaluation because the predicted vibration data can be used to detect, locate and quantify the extent of the cracks or damages in a structure. The problem of vibrational behavior of cracked composite plates has been extensively discussed in the last years [3–9]. However, a few of them [7–9] focus on the damage of matrix cracking which may be initiated as the first damage mode when the plate is subjected to tension or bending load [10, 11]. A test and prediction of natural frequencies of matrix-cracked square laminated plate were presented by Moon et al. [7]. In their analysis, the matrix crack was assumed to be located at 90-ply of the plate, and the reduction in laminate stiffness was derived based on a shear-lag model. Umesh and Ganguli [8] studied the vibration control of a cantilevered smart laminated plate with matrix cracks. The reduced stiffness for the plate with matrix cracks was obtained by using the self-consistent method. They found that the matrix cracks could reduce the natural frequency and the deflection for free and forced vibration, respectively. Adali and Makins [9] investigated the vibration characteristics

of unsymmetric cross-ply laminated plate with matrix cracks. In their studies, the crack was modeled by a self-consistent method. They found that the effect of matrix crack located at the 90-ply was more significant on the linear frequencies than the same matrix crack located at the 0-ply. It is worth noting that in all the above studies, the classical laminate thin plate theory was adopted. The effect of transverse shear deformation is neglected in the classical thin plate theory based on the Kirchhoff hypothesis. Due to low transverse shear modulus relative to the in-plane Young's modulus, transverse shear deformations play a much important role in the kinematics of composite laminates. Neglecting the transverse shear effects and rotary inertia yields incorrect results even for the thin composite laminated plates when the ratio of the two in-plane Young's moduli of a lamina is more than 25 [12]. To account for the effect of transverse shear deformation in plates, several higher-order shear deformation plate theories have been developed, and the major difference of these higher-order shear deformation plate theories lies in that they use different shape functions in the displacement field. Reddy [13] developed a simple higher-order shear deformation plate theory. This theory not only allows parabolic variation of transverse shear strains but also satisfies the condition of the vanishing of transverse shear stresses at the top and bottom surface of the plate. Unlike the first-order shear deformation theory, no shear correction factors are required in this higher-order shear deformation theory, though there are the same numbers of independent unknowns in both the theories.

In the previous works, numerous models focus on the cases of cross-ply laminated plates with cracks only at 90-ply [14] and usually focus on the cases of cross-ply laminated plates with symmetric layup. For a cross-ply laminated plate, the matrix cracks may occur in both 0- and 90-ply. This is called doubly periodic matrix cracking [15, 16]. A number of models have been proposed to predict the stiffness reduction for this matrix cracking, for example self-consistent approach [17–19], variational principles [20–22] and equivalent constraint model [23–25]. As a simple and analytical way, the self-consistent method is applicable to the laminated plates with any kinds of cross-ply layup under different kinds of loading conditions.

Carbon nanotubes (CNTs) have shown the potential to become the important constituent of a new generation of composite materials, by virtue of their superior

mechanical, thermal and electrical properties [26]. One of the potential applications of CNTRCs is in microelectromechanical systems (MEMS) and nanoelectromechanical systems (NEMS) where CNTRCs can be used as key structural components [27]. Compared with the conventional carbon fiber-reinforced laminates, carbon nanotube-reinforced composites (CNTRCs) have the potential of significantly better strength and stiffness. The reinforcement effect of CNTs can be maximized if the CNTs are aligned in a given direction. This can be achieved as reported in recent publications [28, 29]. Several studies have been reported on the linear and nonlinear vibration of functionally graded CNTRC plates [30–34]. They found that a small percentage of nanotube reinforcement leads to significant improvements in plate vibration characteristics. The nonlinear vibration behaviors of a matrix-cracked hybrid laminated beam which contains CNTRC layers and resting on elastic foundations in thermal environments were recently studied by Fan and Wang [35]. In their analysis, a refined shear-lag model was adopted. Their results showed that the crack density plays an important role in the linear vibration of the hybrid laminated beam, but the effect of crack density is less pronounced on the nonlinear-to-linear frequency ratios of the same beam.

In the present work, the nonlinear free and forced vibrations of matrix-cracked hybrid laminated plates containing CNTRC layers resting on elastic foundations in thermal environments are investigated. The novelty of present work is to introduce the matrix cracking in both FRC and CNTRC layers. Unlike in [35], a self-consistent model instead of a refined shear-lag model is used to describe the stiffness reduction in plate due to the matrix cracks. Motion equations are derived based on Reddy's higher-order shear deformation plate theory and solved by means of a two-step perturbation approach. The plate–foundation interaction and thermal effects are both taken into account, and the material properties of both FRC layers and CNTRC layers are assumed to be temperature dependent. The numerical illustrations show the effects of matrix cracks on the nonlinear dynamic responses of hybrid laminated plates under different conditions.

## 2 Self-consistent method for modeling

On the macroscale, the cracked unidirectional composite laminates can be regarded as an orthotropic homoge-

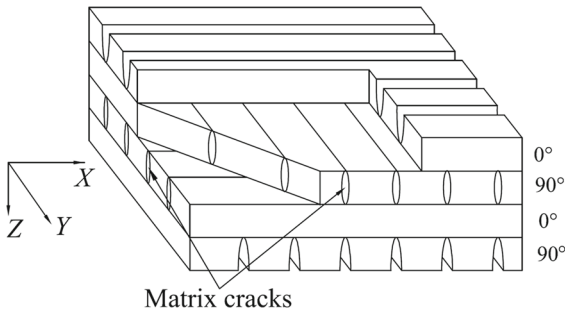


**Fig. 1** Geometry of a cross-ply laminate and the distribution of matrix cracks

neous solid as shown in Fig. 1. The elastic properties of the matrix are identical with those of the fibrous composite and can be easily evaluated. When cracks are introduced, the macroscopic or overall elastic moduli of the solid may change. To make the concept of overall moduli meaningful, it is necessary to consider overall uniform loading. Thus, we introduce uniform overall average stresses  $\bar{\sigma}$  and strains  $\bar{\epsilon}$ , with components arranged in column vectors and related by constitutive equations

$$\bar{\epsilon} = S\bar{\sigma} \tag{1}$$

where  $S$  is the overall compliance matrix of the cracked composite.

Since we are concerned only with a 2-phase model (in which the intact composite is the matrix), here we use the subscript 0 to denote the properties of the intact composite. Following [36], the self-consistent estimates for the overall stiffness and compliance matrices can be expressed by

$$S = S_0 + \bar{\rho}_{crk} \Lambda \tag{2}$$

where

$$\bar{\rho}_{crk} = \frac{1}{4} \pi \rho_{crk} \tag{3}$$

in which the detailed expression of the crack density parameter  $\rho_{crk}$  is defined as [18]

$$\rho_{crk} = 4\eta l^2 \tag{4}$$

where  $\eta$  is the number of cracks per unite area and  $l$  is the half length of two adjacent cracks. Note that the surface layer containing cracks may be regarded as half of a layer of the thickness. This means the crack density of a surface layer is twice as much as that of interior layer with the same angle-ply. The coordinate system presented is different from that used in [36], in which

the fiber is aligned in the  $Z$ -direction, whereas in the present work the fiber is aligned in the  $X$ -direction, as shown in Fig. 1. Accordingly, the matrix  $\Lambda$  has three nonzero components, which are expressed in terms of compliances  $S_{ij}$  of effective medium as

$$\Lambda_{22} = \frac{S_{11}S_{22} - S_{12}^2}{S_{11}}(\sqrt{\alpha_1} + \sqrt{\alpha_2}) \tag{5}$$

$$\Lambda_{44} = \frac{\sqrt{(S_{11}S_{22} - S_{12}^2)(S_{11}S_{33} - S_{13}^2)}}{S_{11}}(\sqrt{\alpha_1} + \sqrt{\alpha_2}) \tag{6}$$

$$\Lambda_{66} = \sqrt{S_{55}S_{66}} \tag{7}$$

where  $\alpha_1$  and  $\alpha_2$  are roots of

$$(S_{11}S_{22} - S_{12}^2)\alpha^2 - [S_{11}S_{44} + 2(S_{11}S_{23} - S_{12}S_{13})]\alpha + S_{11}S_{33} - S_{13}^2 = 0 \tag{8}$$

These results imply that only three compliance coefficients  $S_{22}$ ,  $S_{44}$  and  $S_{66}$  are affected by the cracks.  $S_{66}$  can be obtained from Eqs. (2) and (7), while Eq. (8) can be solved by Newton–Raphson method as reported in [18]. In Eqs. (5)–(8), the compliance matrix  $\bar{S}$  can be expressed as

$$\begin{bmatrix} \bar{S}_{11} \\ \bar{S}_{12} \\ \bar{S}_{22} \\ \bar{S}_{16} \\ \bar{S}_{26} \\ \bar{S}_{66} \end{bmatrix} = \begin{bmatrix} c^4 & 2s^2c^2 & s^4 & s^2c^2 \\ s^2c^2 & 1 - 2s^2c^2 & s^2c^2 & -s^2c^2 \\ s^4 & 2s^2c^2 & c^4 & s^2c^2 \\ 2sc^3 & 2sc(s^2 - c^2) & -2s^3c & sc(s^2 - c^2) \\ 2s^3c & 2sc(c^2 - s^2) & -2s^3c & sc(c^2 - s^2) \\ 4s^2c^2 & -8s^2c^2 & 4s^2c^2 & 1 - 4s^2c^2 \end{bmatrix} \times \begin{bmatrix} S_{11} \\ S_{12} \\ S_{22} \\ S_{66} \end{bmatrix} \tag{9}$$

where

$$c = \cos \theta, s = \sin \theta \tag{10}$$

where  $\theta$  is the lamination angle with respect to the direction of  $X$ -axis. The relationships between stiffness coefficients  $\bar{Q}_{ij}$  and compliance coefficients  $\bar{S}_{ij}$  are

$$\begin{aligned} \bar{Q}_{11} &= \frac{\bar{S}_{22}}{\bar{S}_{11}\bar{S}_{22} - \bar{S}_{12}^2}, \bar{Q}_{12} = -\frac{\bar{S}_{12}}{\bar{S}_{11}\bar{S}_{22} - \bar{S}_{12}^2}, \bar{Q}_{22} \\ &= \frac{\bar{S}_{11}}{\bar{S}_{11}\bar{S}_{22} - \bar{S}_{12}^2} \\ \bar{Q}_{44} &= \frac{1}{\bar{S}_{44}}, \bar{Q}_{55} = \frac{1}{\bar{S}_{55}}, \bar{Q}_{66} = \frac{1}{\bar{S}_{66}} \end{aligned} \tag{11}$$

Since we consider cross-ply laminated plate here, only 0-plyes and 90-plyes are needed to be taken into account.

### 2.1 Material properties of FRC 90-plyies

It is assumed that the 90-plyies are made of FRCs and the material properties of a FRC layer can be expressed as follows [37]

$$\begin{aligned}
 E_{11} &= V_f E_{11}^f + V_m E^m, \\
 \frac{1}{E_{22}} &= \frac{V_f}{E_{22}^f} + \frac{V_m}{E^m} \\
 &\quad - V_f V_m \frac{V_f^2 E^m / E_{22}^f + V_m^2 E_{22}^f / E^m - 2v^f v^m}{V_f E_{22}^f + V_m E^m}, \\
 \frac{1}{G_{ij}} &= \frac{V_f}{G_{ij}^f} + \frac{V_m}{G^m} \quad (ij = 12, 13 \text{ and } 23) \\
 \rho &= V_f \rho^f + V_m \rho^m, \\
 v_{12} &= V_f v^f + V_m v^m, \tag{12}
 \end{aligned}$$

where  $E_{11}^f, E_{22}^f, G_{12}^f, G_{13}^f, G_{23}^f$  and  $v^f$  are the Young’s moduli, shear moduli and Poisson’s ratio, respectively, of the fiber, while  $E^m, G^m$  and  $v^m$  are corresponding properties for the matrix.  $\rho^f, \rho^m$  and  $\rho$  are the mass densities of the fiber, matrix and the ply.  $V_f$  and  $V_m$  are the fiber and matrix volume fractions and are related by  $V_f + V_m = 1$ .

### 2.2 Material properties of CNTRC 0-plyies

The 0-plyies are assumed to be made of CNTRCs. Based on extended rule of mixture, the effective properties of CNTRC plyies can be defined by [38]

$$\begin{aligned}
 E_{11} &= \eta_1 V_{CN} E_{11}^{CN} + V_m E^m, \\
 \frac{\eta_2}{E_{22}} &= \frac{V_{CN}}{E_{22}^{CN}} + \frac{V_m}{E^m}, \\
 \frac{\eta_3}{G_{12}} &= \frac{V_{CN}}{G_{12}^{CN}} + \frac{V_m}{G^m}, \\
 \rho &= V_{CN} \rho^{CN} + V_m \rho^m, \\
 v_{12} &= V_{CN}^* v_{12}^{CN} + V_m v^m, \tag{13}
 \end{aligned}$$

in which  $E_{11}^{CN}, E_{22}^{CN}, G_{12}^{CN}, v_{12}^{CN}$  and  $\rho^{CN}$  are the Young’s and shear moduli, Poisson’s ratio and mass density of the single-walled carbon nanotubes (SWCNTs), respectively.  $\eta_j (j = 1, 2, 3)$  are the CNT efficiency parameters, and  $V_{CN}$  is the volume fraction of the CNT, which satisfies the relationship of  $V_{CN} + V_m = 1$ . Two types of FG-CNTRCs, i.e., FG-V, and FG- $\Lambda$ , as defined in [39] are considered. The corresponding volume fraction  $V_{CN}$  for each type is

$$\begin{aligned}
 V_{CN} &= 2 \left( \frac{Z - t_0}{t_1 - t_0} \right) V_{CN}^* \quad (\text{FG-V}), \\
 V_{CN} &= 2 \left( \frac{t_1 - Z}{t_1 - t_0} \right) V_{CN}^* \quad (\text{FG} - \Lambda), \tag{14}
 \end{aligned}$$

in which  $Z = t_1$  and  $Z = t_0$ , respectively, denote the values in Z-direction at the top surface and bottom surface of a 0-ply. In Eq. (14),  $V_{CN}^*$  depends on the mass densities of CNTs and matrix, and the detailed definition is

$$V_{CN}^* = \frac{w_{CN}}{w_{CN} + (\rho^{CN} / \rho^m) - (\rho^{CN} / \rho^m) w_{CN}} \tag{15}$$

in which  $w_{CN}$  is the mass fraction of SWCNTs. For UD-CNTRC 0-plyies,  $V_{CN}$  is equal to  $V_{CN}^*$ .

In the longitudinal and transverse directions, the thermal expansion coefficients  $\alpha_{11}$  and  $\alpha_{22}$  for an arbitrary layer can be expressed by [40]

$$\begin{aligned}
 \alpha_{11} &= \frac{V_i E_{11}^i \alpha_{11}^i + V_m E^m \alpha_m}{V_i E_{11}^i + V_m E^m} \quad (i = f \text{ or } CN), \\
 \alpha_{22} &= \left( 1 + v_{12}^i \right) V_i \alpha_{22}^i + \left( 1 + v^m \right) V_m \alpha^m \\
 &\quad - v_{12} \alpha_{11} \quad (i = f \text{ or } CN), \tag{16}
 \end{aligned}$$

in which  $\alpha_{11}^i, \alpha_{22}^i (i = f \text{ or } CN)$  and  $\alpha^m$  are thermal expansion coefficients, respectively, of the carbon fiber (or carbon nanotube) and the matrix.

The material properties of carbon nanotube and matrix are assumed to be functions of temperature, so that the effective material properties of both FRC and CNTRC plyies are functions of temperature.

### 3 Motion equations of hybrid laminated plate

It is assumed that a laminated plate with length  $a$ , width  $b$  and thickness  $h$  rests on an elastomeric substrate with finite depth. This substrate may be modeled as an elastic foundation of Pasternak type. The plate and foundation are assumed to be bonded perfectly, that is, the plate and foundation are not separated after the deformation occurs. This is truly an ideal state. The coupling effect of plate and foundation can be expressed by an interaction force

$$p(X, Y) = \bar{K}_1 \bar{W} - \bar{K}_2 \nabla^2 \bar{W} \tag{17}$$

in which  $p$  is the force per unit area,  $\nabla^2$  is Laplace operator,  $\bar{K}_1$  is the Winkler stiffness, and  $\bar{K}_2$  is the shearing

layer stiffness of the foundation. The material of elastomeric substrate is assumed to be temperature dependent. Hence, the Winkler stiffness may be expressed by [41]:

$$\bar{K}_1 = \frac{E_F [5 - (2\gamma_1^2 + 6\gamma_1 + 5) \exp(-2\gamma_1)]}{4b(1 - \nu_0^2)(2 - c_1)^2} \quad (18)$$

where  $c_1 = (\gamma_1 + 2) \exp(-\gamma_1)$ ,  $\gamma_1 = H_s/b$ ,  $E_F = E_s/(1 - \nu_s^2)$  and  $\nu_0 = \nu_s/(1 - \nu_s)$ , in which  $E_s$  and  $\nu_s$  are Young’s modulus and Poisson’s ratio of the foundation, respectively, and  $H_s$  is the depth of the foundation. The shear layer stiffness  $\bar{K}_2$  is assumed to be one-tenth of the Winkler stiffness  $\bar{K}_1$ . The initial and additional deflections are expressed by  $\bar{W}^*(X, Y)$  and  $\bar{W}(X, Y)$ , respectively. The plate is exposed to elevated temperature and is subjected to a transverse dynamic load  $Q(X, Y, t)$ . Based on Reddy’s higher-order shear deformation theory with a von Kármán type of kinematic nonlinearity, Shen [42] derived a set of general von Kármán-type equations which can be expressed in terms of a transverse displacement  $\bar{W}$ , two rotations  $\bar{\Psi}_x$  and  $\bar{\Psi}_y$ , and stress function  $\bar{F}$  as defined by

$$\bar{N}_X = \frac{\partial^2 \bar{F}}{\partial Y^2}, \bar{N}_Y = \frac{\partial^2 \bar{F}}{\partial X^2}, \bar{N}_{XY} = -\frac{\partial^2 \bar{F}}{\partial X \partial Y} \quad (19)$$

where  $\bar{N}_X$ ,  $\bar{N}_Y$  and  $\bar{N}_{XY}$  are stress resultants.

These equations can be expressed by [12]

$$\begin{aligned} \tilde{L}_{11}(\bar{W}) - \tilde{L}_{12}(\bar{\Psi}_x) - \tilde{L}_{13}(\bar{\Psi}_y) + \tilde{L}_{14}(\bar{F}) \\ - \tilde{L}_{15}(\bar{N}^T) - \tilde{L}_{16}(\bar{M}^T) \\ = \tilde{L}(\bar{W}, \bar{F}) + \tilde{L}_{17}(\ddot{\bar{W}}) + I_8(\ddot{\bar{\Psi}}_{x,x} + \ddot{\bar{\Psi}}_{y,y}) \\ - (\bar{K}_1 \bar{W} - \bar{K}_2 \nabla^2 \bar{W}) + Q \end{aligned} \quad (20)$$

$$\begin{aligned} \tilde{L}_{21}(\bar{F}) + \tilde{L}_{22}(\bar{\Psi}_x) + \tilde{L}_{23}(\bar{\Psi}_y) \\ - \tilde{L}_{24}(\bar{W}) - \tilde{L}_{25}(\bar{N}^T) = -\frac{1}{2} \tilde{L}(\bar{W}, \bar{W}) \end{aligned} \quad (21)$$

$$\begin{aligned} \tilde{L}_{31}(\bar{W}) + \tilde{L}_{32}(\bar{\Psi}_x) - \tilde{L}_{33}(\bar{\Psi}_y) + \tilde{L}_{34}(\bar{F}) \\ - \tilde{L}_{35}(\bar{N}^T) - \tilde{L}_{36}(\bar{S}^T) = I_9 \ddot{\bar{W}}_{,x} + I_{10} \ddot{\bar{\Psi}}_x \end{aligned} \quad (22)$$

$$\begin{aligned} \tilde{L}_{41}(\bar{W}) - \tilde{L}_{42}(\bar{\Psi}_x) + \tilde{L}_{43}(\bar{\Psi}_y) + \tilde{L}_{44}(\bar{F}) \\ - \tilde{L}_{45}(\bar{N}^T) - \tilde{L}_{46}(\bar{S}^T) = I_9 \ddot{\bar{W}}_{,y} + I_{10} \ddot{\bar{\Psi}}_y \end{aligned} \quad (23)$$

in which the linear operators  $\tilde{L}_{ij}(\cdot)$  and the nonlinear operators  $L_{ij}(\cdot)$  are defined as in [12].  $I_i$  are defined in Eqs. (31) and (32) below. In the above equations, the superposed dots indicate differentiation with respect to time  $t$ . It has been reported that von Kármán-type nonlinearity is accurate for flexural vibration analysis of laminated plates [43]. In the frame work of

HSDT, both Green-Lagrange and von Kármán strain-displacement relationships may be used. The complete Green-Lagrange strain expressions make the governing equations nonlinear in all the displacement parameters of the plate. The Green-Lagrange strain expressions are particularly applicable for in-plane vibrational problem [44, 45], whereas the von Kármán strain expressions are simple and convenient to derive governing equations of  $\bar{W} - \bar{F}$  type which are particularly applicable for a mixed boundary value problem.

Considering the effects of thermal environment, the constitutive relations of the plate are

$$\begin{bmatrix} \bar{N} \\ \bar{M} \\ \bar{P} \end{bmatrix} = \begin{bmatrix} A & B & E \\ B & D & F \\ E & F & H \end{bmatrix} \begin{bmatrix} \epsilon^0 \\ \kappa^0 \\ \kappa^2 \end{bmatrix} + \begin{bmatrix} \bar{N}^T \\ \bar{M}^T \\ \bar{P}^T \end{bmatrix} \quad (24a)$$

$$\begin{bmatrix} \bar{Q} \\ \bar{R} \end{bmatrix} = \begin{bmatrix} A & D \\ D & F \end{bmatrix} \begin{bmatrix} \epsilon^0 \\ \kappa^2 \end{bmatrix} \quad (24b)$$

where  $A, B, D$ , etc., are plate stiffness, and the detailed definition can be found in Eq. (30) below.  $\epsilon^0$  is the strain of mid-plane, while  $\kappa^0$  and  $\kappa^2$  are curvatures of mid-plane.  $\bar{N}^T, \bar{M}^T$  and  $\bar{P}^T$  are the thermal forces, moments and higher-order moments caused by the temperature change  $\Delta T(X, Y, Z)$  and are defined by

$$\begin{bmatrix} \bar{N}_x^T \\ \bar{N}_y^T \\ \bar{N}_{xy}^T \\ \bar{M}_x^T \\ \bar{M}_y^T \\ \bar{M}_{xy}^T \\ \bar{P}_x^T \\ \bar{P}_y^T \\ \bar{P}_{xy}^T \end{bmatrix} = \sum_{i=1}^N \int_{h_{k-1}}^{h_k} \begin{bmatrix} A_x \\ A_y \\ A_{xy} \end{bmatrix}_k (1, Z, Z^2) \Delta T dZ \quad (25a)$$

$$\begin{bmatrix} \bar{S}_x^T \\ \bar{S}_y^T \\ \bar{S}_{xy}^T \end{bmatrix} = \begin{bmatrix} \bar{M}_x^T \\ \bar{M}_y^T \\ \bar{M}_{xy}^T \end{bmatrix} - \frac{4}{3h^2} \begin{bmatrix} \bar{P}_x^T \\ \bar{P}_y^T \\ \bar{P}_{xy}^T \end{bmatrix} \quad (25b)$$

In Eq. (25a),

$$\begin{bmatrix} A_x \\ A_y \\ A_{xy} \end{bmatrix} = - \begin{bmatrix} \bar{Q}_{11} & \bar{Q}_{12} & \bar{Q}_{16} \\ \bar{Q}_{12} & \bar{Q}_{22} & \bar{Q}_{26} \\ \bar{Q}_{16} & \bar{Q}_{26} & \bar{Q}_{66} \end{bmatrix} \begin{bmatrix} c^2 & s^2 \\ s^2 & c^2 \\ 2cs & -2cs \end{bmatrix} \times \begin{bmatrix} \alpha_{11} \\ \alpha_{22} \end{bmatrix} \quad (26)$$

in which  $\alpha_{11}$  and  $\alpha_{22}$  are thermal expansion coefficients of  $k$ th layer in longitudinal and transverse directions.

Partly inverting Eq. (24a), we obtain

$$\begin{bmatrix} \epsilon^0 \\ M^* \\ P^* \end{bmatrix} = \begin{bmatrix} A^* & B^* & E^* \\ -(B^*)^T & D^* & (F^*)^T \\ -(E^*)^T & F^* & H^* \end{bmatrix} \begin{bmatrix} N^* \\ \kappa^0 \\ \kappa^2 \end{bmatrix} \quad (27)$$

where the superscript T represents transpose of matrix, and

$$N^* = \bar{N} - \bar{N}^T, M^* = \bar{M} - \bar{M}^T, P^* = \bar{P} - \bar{P}^T \tag{28}$$

The reduced matrices  $A^*$ ,  $B^*$ , etc., are defined by

$$\begin{aligned} A^* &= A^{-1}, B^* = -A^{-1}B, D^* = D - BA^{-1}B, E^* \\ &= -A^{-1}E \\ F^* &= F - EA^{-1}B, H^* = H - EA^{-1}E \end{aligned} \tag{29}$$

Generally,  $A^*$ ,  $D^*$  and  $H^*$  are symmetric matrices, while  $B^*$ ,  $E^*$  and  $F^*$  may not always be. The plate stiffnesses  $A_{ij}$ ,  $B_{ij}$ ,  $D_{ij}$ , etc., are defined as

$$\begin{aligned} &(A_{ij}, B_{ij}, D_{ij}, E_{ij}, F_{ij}, H_{ij}) \\ &= \sum_{k=1}^N \int_{h_{k-1}}^{h_k} (\bar{Q}_{ij})_k(1, Z, Z^2, Z^3, Z^4, Z^6)dZ, \\ &(i, j = 1, 2, 6) \end{aligned} \tag{30a}$$

$$\begin{aligned} &(A_{ij}, D_{ij}, F_{ij}) = \sum_{k=1}^N \int_{h_{k-1}}^{h_k} (\bar{Q}_{ij})_k(1, Z^2, Z^4)dZ, \\ &(i, j = 4, 5) \end{aligned} \tag{30b}$$

and the generalized inertia  $I_i$  ( $i = 1, 2, 3, 4, 5, 7$ ) is defined as

$$\begin{aligned} &(I_1, I_2, I_3, I_4, I_5, I_7) \\ &= \sum_{k=1}^N \int_{h_{k-1}}^{h_k} \rho_k(1, Z, Z^2, Z^3, Z^4, Z^6)dZ \end{aligned} \tag{31}$$

and

$$\begin{aligned} \bar{I}_2 &= I_2 - \frac{4}{3h^2}I_4, \bar{I}_5 = I_5 - \frac{4}{3h^2}I_7, \bar{I}_3 \\ &= I_3 - \frac{8}{3h^2}I_5 + \frac{16}{9h^4}I_7 \\ I_8 &= \frac{I_2\bar{I}_2}{I_1} - \bar{I}_3 - \frac{4}{3h^2}\bar{I}_5, I_9 = \frac{4}{3h^2}\left(\bar{I}_5 - \frac{\bar{I}_2I_4}{I_1}\right), \\ I_{10} &= \frac{\bar{I}_2\bar{I}_2}{I_1} - \bar{I}_3 \end{aligned} \tag{32}$$

It is assumed that four edges of plate are simply supported. Based on the in-plane behavior at the edges, two cases of boundary conditions (immovable edges and movable edges) are considered

$$X = 0, a; \quad \bar{W} = \bar{\Psi}_y = 0 \tag{33a}$$

$$\bar{M}_x = \bar{P}_x = 0 \tag{33b}$$

$$\int_0^b \bar{N}_x dY = 0 \text{ (movable)} \tag{33c}$$

$$\bar{U} = 0 \text{ (immovable)} \tag{33d}$$

$Y = 0, b;$

$$\bar{W} = \bar{\Psi}_x = 0 \tag{33e}$$

$$\bar{M}_y = \bar{P}_y = 0 \tag{33f}$$

$$\int_0^b \bar{N}_y dX = 0 \text{ (movable)} \tag{33g}$$

$$\bar{V} = 0 \text{ (immovable)} \tag{33h}$$

In Eq. (33), the in-plane immovable conditions of Eqs. (33d) and (33h) can be expressed, respectively, by

$$\begin{aligned} &\int_0^b \int_0^a \left\{ A_{11}^* \frac{\partial^2 \bar{F}}{\partial Y^2} + A_{12}^* \frac{\partial^2 \bar{F}}{\partial X^2} \right. \\ &+ \left[ \left( B_{11}^* - \frac{4}{3h^2}E_{11}^* \right) \frac{\partial \bar{\Psi}_x}{\partial X} + \left( B_{12}^* - \frac{4}{3h^2}E_{12}^* \right) \frac{\partial \bar{\Psi}_y}{\partial Y} \right] \\ &- \frac{4}{3h^2} \left( E_{11}^* \frac{\partial^2 \bar{W}}{\partial X^2} + E_{12}^* \frac{\partial^2 \bar{W}}{\partial Y^2} \right) - \frac{1}{2} \left( \frac{\partial \bar{W}}{\partial X} \right)^2 \\ &\left. - (A_{11}^* \bar{N}_x^T + A_{12}^* \bar{N}_y^T) \right\} dXdY = 0 \end{aligned} \tag{34a}$$

$$\begin{aligned} &\int_0^a \int_0^b \left\{ A_{22}^* \frac{\partial^2 \bar{F}}{\partial X^2} + A_{12}^* \frac{\partial^2 \bar{F}}{\partial Y^2} \right. \\ &+ \left[ \left( B_{21}^* - \frac{4}{3h^2}E_{21}^* \right) \frac{\partial \bar{\Psi}_x}{\partial X} + \left( B_{22}^* - \frac{4}{3h^2}E_{22}^* \right) \frac{\partial \bar{\Psi}_y}{\partial Y} \right] \\ &- \frac{4}{3h^2} \left( E_{21}^* \frac{\partial^2 \bar{W}}{\partial X^2} + E_{22}^* \frac{\partial^2 \bar{W}}{\partial Y^2} \right) - \frac{1}{2} \left( \frac{\partial \bar{W}}{\partial Y} \right)^2 \\ &\left. - (A_{12}^* \bar{N}_x^T + A_{22}^* \bar{N}_y^T) \right\} dYdX = 0 \end{aligned} \tag{34b}$$

### 4 Solutions for free and forced vibrations

Before carrying out the solution process, it is convenient to first define the following dimensionless quantities for such plates. Introduce dimensionless coefficients

$$\begin{aligned} x &= \pi \frac{X}{a}, y = \pi \frac{Y}{b}, \beta = \frac{a}{b}, \\ W &= \frac{W}{[D_{11}^* D_{22}^* A_{11}^* A_{22}^*]^{1/4}}, F = \frac{\bar{F}}{[D_{11}^* D_{22}^*]^{1/2}}, \\ (\Psi_x, \Psi_y) &= \frac{a}{\pi} \frac{(\bar{\Psi}_x, \bar{\Psi}_y)}{[D_{11}^* D_{22}^* A_{11}^* A_{22}^*]^{1/4}}, \gamma_{14} = \left[ \frac{D_{22}^*}{D_{11}^*} \right]^{1/2}, \end{aligned}$$

$$\begin{aligned} \gamma_{24} &= \left[ \frac{A_{11}^*}{A_{22}^*} \right]^{1/2}, \gamma_5 = -\frac{A_{12}^*}{A_{22}^*}, \\ (\gamma_{T1}, \gamma_{T2}) &= \frac{a^2}{\pi^2} \frac{(A_x^T, A_y^T)}{[D_{11}^* D_{22}^*]^{1/2}}, (\gamma_{T3}, \gamma_{T4}, \gamma_{T6}, \gamma_{T7}) \\ &= \frac{a^2}{\pi^2 h D_{11}^*} \left( D_x^T, D_y^T, \frac{4}{3h^2} F_x^T, \frac{4}{3h^2} F_y^T \right), \\ (K_1, K_2) &= \left( \frac{\bar{K}_1 a^4}{\pi^4 D_{11}^*}, \frac{\bar{K}_2 a^2}{\pi^2 D_{11}^*} \right), (M_x, P_x) \\ &= \frac{a^2}{\pi^2} \frac{(\bar{M}_x, \frac{4}{3h^2} \bar{P}_x)}{D_{11}^* [D_{11}^* D_{22}^* A_{11}^* A_{22}^*]^{1/4}}, \tilde{t} = \frac{\pi t}{a} \sqrt{\frac{E_0}{\rho_0}}, \\ \omega_L &= \Omega_L \frac{a}{\pi} \sqrt{\frac{\rho_0}{E_0}}, \gamma_{170} \\ &= -\frac{I_1 E_0 a^2}{\pi^2 \rho_0 D_{11}^*}, \gamma_{171} = \frac{4E_0(I_5 I_1 - I_4 I_2)}{3\rho_0 h^2 I_1 D_{11}^*} \\ (\gamma_{80}, \gamma_{90}, \gamma_{10}) &= (I_8, I_9, I_{10}) \frac{E_0}{\rho_0 D_{11}^*}, \lambda_q \\ &= \frac{qa^4}{\pi^4 D_{11}^* [D_{11}^* D_{22}^* A_{11}^* A_{22}^*]^{1/4}} \end{aligned} \tag{35}$$

where  $\rho_0$  and  $E_0$  are, respectively, the values of  $\rho^m$  and  $E^m$  at the reference temperature ( $T = 300\text{K}$ ).  $A_x^T, D_x^T, F_x^T$ , etc., are defined by

$$\begin{aligned} \begin{bmatrix} A_x^T & D_x^T & F_x^T \\ A_y^T & D_y^T & F_y^T \end{bmatrix} &= -\sum_{k=1}^n \int_{h_{k-1}}^{h_k} \begin{bmatrix} A_x \\ A_y \end{bmatrix} \\ &(1, Z, Z^3) dZ \end{aligned} \tag{36}$$

where  $A_x$  and  $A_y$  are given in Eq. (26). In uniform temperature field,  $L_{15}(N^T) = L_{25}(N^T) = L_{35}(N^T) = L_{45}(N^T) = 0$ ; then, Eqs. (20)–(23) can be expressed in dimensionless form as

$$\begin{aligned} &L_{11}(W) - L_{12}(\Psi_x) - L_{13}(\Psi_y) \\ &+ \gamma_{14}L_{14}(F) - L_{16}(M^T) \\ &= \gamma_{14}\beta^2 L(W, F) + L_{17}(\ddot{W}) \\ &+ \gamma_{80} \left( \frac{\partial \ddot{\Psi}_x}{\partial x} + \beta \frac{\partial \ddot{\Psi}_y}{\partial y} \right) \\ &- (K_1 W - K_2 \nabla^2 W) + \lambda_q \end{aligned} \tag{37}$$

$$\begin{aligned} &L_{21}(F) + \gamma_{24}L_{22}(\Psi_x) \\ &+ \gamma_{24}L_{23}(\Psi_y) - \gamma_{24}L_{24}(W) \\ &= -\frac{1}{2}\gamma_{24}\beta^2 L(W, W) \end{aligned} \tag{38}$$

$$\begin{aligned} &L_{31}(W) + L_{32}(\Psi_x) - L_{33}(\Psi_y) \\ &+ \gamma_{14}L_{34}(F) - L_{36}(S^T) \end{aligned}$$

$$= \gamma_{90} \frac{\partial \ddot{W}}{\partial x} + \gamma_{10} \ddot{\Psi}_x \tag{39}$$

$$\begin{aligned} &L_{41}(W) - L_{42}(\Psi_x) + L_{43}(\Psi_y) \\ &+ \gamma_{14}L_{44}(F) - L_{46}(S^T) \\ &= \gamma_{90}\beta \frac{\partial \ddot{W}}{\partial y} + \gamma_{10} \ddot{\Psi}_y \end{aligned} \tag{40}$$

in which linear operators  $L_{ij}(\cdot)$  are defined as in [12].

The boundary conditions of Eqs. (33a)–(33h) can be rewritten as

$$\begin{aligned} &x = 0, \pi; \\ &W = \Psi_y = 0 \end{aligned} \tag{41a}$$

$$M_x = P_x = 0 \tag{41b}$$

$$\int_0^\pi \beta^2 \frac{\partial^2 F}{\partial y^2} dy = 0 \text{ (movable)} \tag{41c}$$

$$\begin{aligned} &\int_0^\pi \int_0^\pi \left[ \gamma_{24}^2 \beta^2 \frac{\partial^2 F}{\partial y^2} - \gamma_5 \frac{\partial^2 F}{\partial x^2} \right. \\ &+ \gamma_{24} \left( \gamma_{511} \frac{\partial \Psi_x}{\partial x} + \gamma_{233} \beta \frac{\partial \Psi_y}{\partial y} \right) \\ &- \gamma_{24} \left( \gamma_{611} \frac{\partial^2 W}{\partial x^2} + \gamma_{244} \beta^2 \frac{\partial^2 W}{\partial y^2} \right) \\ &\left. - \frac{1}{2} \gamma_{24} \left( \frac{\partial W}{\partial x} \right)^2 + (\gamma_{24} \gamma_{T1} - \gamma_5 \gamma_{T2}) \Delta T \right] \\ &dx dy = 0 \text{ (immovable)} \end{aligned} \tag{41d}$$

$$y = 0, \pi;$$

$$W = \Psi_x = 0 \tag{41e}$$

$$M_y = P_y = 0 \tag{41f}$$

$$\int_0^\pi \frac{\partial^2 F}{\partial x^2} dx = 0 \text{ (movable)} \tag{41g}$$

$$\begin{aligned} &\int_0^\pi \int_0^\pi \left[ \frac{\partial^2 F}{\partial x^2} - \gamma_5 \beta^2 \frac{\partial^2 F}{\partial y^2} \right. \\ &+ \gamma_{24} \left( \gamma_{220} \frac{\partial \Psi_x}{\partial x} + \gamma_{522} \beta \frac{\partial \Psi_y}{\partial y} \right) \\ &- \gamma_{24} \left( \gamma_{240} \frac{\partial^2 W}{\partial x^2} + \gamma_{622} \beta^2 \frac{\partial^2 W}{\partial y^2} \right) \\ &\left. - \frac{1}{2} \gamma_{24} \beta^2 \left( \frac{\partial W}{\partial y} \right)^2 + (\gamma_{T2} - \gamma_5 \gamma_{T1}) \Delta T \right] \\ &dy dx = 0 \text{ (immovable)} \end{aligned} \tag{41h}$$

Equations (37)–(40) can be solved by means of a two-step perturbation technique [12]. Because bending–stretching coupling exists in functionally graded CNTRC 0-ply, the initial deflection caused by thermal bending moments should be determined firstly.

It is assumed that the solutions of Eqs. (37)–(40) are

$$\begin{aligned}
 W(x, y, \tilde{t}) &= W^*(x, y) + \tilde{W}(x, y, \tilde{t}) \\
 \Psi_x(x, y, \tilde{t}) &= \Psi_x^*(x, y) + \tilde{\Psi}_x(x, y, \tilde{t}) \\
 \Psi_y(x, y, \tilde{t}) &= \Psi_y^*(x, y) + \tilde{\Psi}_y(x, y, \tilde{t}) \\
 F(x, y, \tilde{t}) &= F^*(x, y) + \tilde{F}(x, y, \tilde{t})
 \end{aligned} \tag{42}$$

in which  $W^*(x, y)$  is initial deflection caused by thermal bending moments and  $\tilde{W}(x, y, \tilde{t})$  is additional dynamic deflection.  $\Psi_x^*(x, y)$ ,  $\Psi_y^*(x, y)$  and  $F^*(x, y)$  are rotations and stress function corresponding to  $W^*(x, y)$ , while  $\tilde{\Psi}_x(x, y, \tilde{t})$ ,  $\tilde{\Psi}_y(x, y, \tilde{t})$  and  $\tilde{F}(x, y, \tilde{t})$  corresponding to  $\tilde{W}(x, y, \tilde{t})$  have the similar definitions as  $\Psi_x^*(x, y)$ ,  $\Psi_y^*(x, y)$  and  $F^*(x, y)$ . For the conditions of in-plane movable ends,  $W^*(x, y) = \Psi_x^*(x, y) = \Psi_y^*(x, y) = F^*(x, y) = 0$ , while for the conditions of in-plane immovable ends,  $W^*(x, y)$ ,  $\Psi_x^*(x, y)$ ,  $\Psi_y^*(x, y)$  and  $F^*(x, y)$  should satisfy non-linear thermal bending equations. The second set of equations gives the homogeneous solution of vibration characteristics on the initial deflected plate that can be expressed by

$$\begin{aligned}
 \tilde{W}(x, y, \tilde{t}) &= \varepsilon \left[ A_{11}^{(1)}(\tilde{t}) \sin mx \sin ny \right] \\
 &+ \varepsilon^3 \left[ A_{11}^{(3)}(\tilde{t}) \sin mx \sin my \right. \\
 &+ A_{31}^{(3)}(\tilde{t}) \sin 3mx \sin ny \\
 &\left. + A_{13}^{(3)}(\tilde{t}) \sin mx \sin 3ny \right] + O(\varepsilon^4)
 \end{aligned} \tag{43}$$

$$\begin{aligned}
 \tilde{F}(x, y, \tilde{t}) &= -B_{00}^{(0)} y^2 / 2 - b_{00}^{(0)} x^2 / 2 \\
 &+ \varepsilon \left[ B_{11}^{(1)}(\tilde{t}) + \ddot{B}_{11}^{(3)}(\tilde{t}) \right] \sin mx \sin ny \\
 &+ \varepsilon \left[ -B_{00}^{(2)} y^2 / 2 - b_{00}^{(2)} x^2 / 2 + B_{02}^{(2)}(\tilde{t}) \cos 2ny \right. \\
 &\left. + B_{20}^{(2)}(\tilde{t}) \cos 2mx \right] \\
 &+ \varepsilon^3 \left[ -B_{00}^{(2)} y^2 / 2 - b_{00}^{(2)} x^2 / 2 + B_{02}^{(2)}(\tilde{t}) \cos 2ny \right. \\
 &\left. + B_{20}^{(2)}(\tilde{t}) \cos 2mx \right] \\
 &+ O(\varepsilon^4)
 \end{aligned} \tag{44}$$

$$\begin{aligned}
 \tilde{\Psi}_x(x, y, \tilde{t}) &= \varepsilon \left[ C_{11}^{(1)}(\tilde{t}) + \ddot{C}_{11}^{(3)}(\tilde{t}) \right] \\
 &\times \cos mx \sin ny + \varepsilon^2 C_{20}^{(2)}(\tilde{t}) \sin 2mx \\
 &+ \varepsilon^3 \left[ D_{31}^{(3)}(\tilde{t}) \cos 3mx \sin ny \right. \\
 &\left. + D_{13}^{(3)}(\tilde{t}) \cos mx \sin 3ny \right] + O(\varepsilon^4)
 \end{aligned} \tag{45}$$

$$\begin{aligned}
 \tilde{\Psi}_y(x, y, \tilde{t}) &= \varepsilon \left[ D_{11}^{(1)}(\tilde{t}) + \ddot{D}_{11}^{(3)}(\tilde{t}) \right] \\
 &\sin mx \cos ny + \varepsilon^2 D_{02}^{(2)}(\tilde{t}) \sin 2ny \\
 &+ \varepsilon^3 \left[ D_{31}^{(3)}(\tilde{t}) \sin 3mx \cos ny \right. \\
 &\left. + D_{13}^{(3)}(\tilde{t}) \sin mx \cos 3ny \right] + O(\varepsilon^4)
 \end{aligned} \tag{46}$$

$$\begin{aligned}
 \lambda_q(x, y, \tilde{t}) &= \varepsilon \left[ g_1 A_{11}^{(1)}(\tilde{t}) + g_4 \ddot{A}_{11}^{(1)}(\tilde{t}) \right] \\
 &\sin mx \sin ny \\
 &+ \left( \varepsilon A_{11}^{(1)}(\tilde{t}) \right)^2 (g_{20} \cos 2mx + g_{02} \cos 2ny) \\
 &+ \left( \varepsilon A_{11}^{(1)}(\tilde{t}) \right)^3 g_3 \sin mx \sin ny + O(\varepsilon^4)
 \end{aligned} \tag{47}$$

It is worth noting that  $t$  has been replaced back by  $\tilde{t}$  in Eqs. (43)–(47), and all coefficients can be expressed in form of  $A_{11}^{(1)}(\tilde{t})$ . In Eq. (44),  $B_{00}^{(0)}$ ,  $b_{00}^{(0)}$ ,  $B_{00}^{(2)}$  and  $b_{00}^{(2)}$  are zero-valued when ends are movable, but when ends are immovable, they can be obtained by solving Eqs. (41d) and (41h) and the detailed expressions are given in [31].

In Eq. (47),  $(\varepsilon A_{11}^{(1)})$  is taken as the second perturbation parameter relating to the dimensionless vibration amplitude  $W_m$ . From Eq. (43), taking  $(x, y) = (\pi/2m, \pi/2n)$  yields

$$\varepsilon A_{11}^{(1)} = \tilde{W}_m - \Theta_1 \tilde{W}_m^3 + \dots \tag{48}$$

Substituting Eq. (48) into Eq. (47) and applying Galerkin procedure, for the case of forced vibration, we have

$$\begin{aligned}
 g_{40} \frac{d^2 \left( \varepsilon A_{11}^{(1)} \right)}{d\tilde{t}^2} + g_{41} \left( \varepsilon A_{11}^{(1)} \right) + g_{42} \left( \varepsilon A_{11}^{(1)} \right)^2 \\
 + g_{43} \left( \varepsilon A_{11}^{(1)} \right)^3 = \bar{\lambda}_q
 \end{aligned} \tag{49}$$

in which

$$\bar{\lambda}_q(\tilde{t}) = \frac{4}{\pi^2} \int_0^\pi \int_0^\pi \lambda_q(x, y, \tilde{t}) \sin mx \sin ny dx dy \tag{50}$$

All symbols used in Eqs. (43)–(49) are described in detail in ‘‘Appendix’’. If zero-valued initial conditions prevail, i.e.,  $\tilde{W}_m(0) = \dot{\tilde{W}}_m(0) = 0$ , Eq. (49) may then be solved by using the Runge–Kutta method [46]. Substituting these solved solutions back into Eqs. (43)–(46), we obtain both displacements and stress function of the plate.



For the case of free vibration, we have  $\lambda_q=0$ . That is,

$$\bar{\lambda}_q(\tilde{t}) = \frac{4}{\pi^2} \int_0^\pi \int_0^\pi \lambda_q(x, y, \tilde{t}) \times \sin mx \sin ny dx dy = 0 \tag{51}$$

In this case, Eq. (49) becomes

$$g_{40} \frac{d^2(\varepsilon A_{11}^{(1)})}{d\tilde{t}^2} + g_{41}(\varepsilon A_{11}^{(1)}) + g_{42}(\varepsilon A_{11}^{(1)})^2 + g_{43}(\varepsilon A_{11}^{(1)})^3 = 0 \tag{52}$$

The solution of Eq. (52) can be written as

$$\omega_{NL} = \omega_L \left[ 1 + \frac{9g_{41}g_{43} - 10g_{42}^2}{12g_{41}^2} A^2 \right]^{1/2} \tag{53}$$

where the dimensionless linear frequency is  $\omega_L = [g_{41}/g_{40}]^{1/2}$ ,  $A$  is the maximal dimensionless deflection of plate, and  $A = W_m = \bar{W}_{\max}/[D_{11}^* D_{22}^* A_{11}^* A_{22}^*]^{1/2}$ .

### 5 Numerical results and discussion

Numerical results are presented in this section for free and forced vibration of hybrid cross-ply laminated plates in thermal environments. First, it is needed to determine the effective material properties of FRCs and CNTRCs. It is assumed that FRCs and CNTRCs have the same matrix material and the mechanical properties of matrix are assumed to be  $\rho^m = 1150 \text{ kg/m}^3$ ,  $\nu^m = 0.34$ ,  $\alpha^m = 45(1 + 0.0005\Delta T) \times 10^{-6} \text{ K}^{-1}$  and  $E^m = (3.52 - 0.0034T) \text{ GPa}$ , in which  $T = T_0 + \Delta T$  and  $T_0 = 300 \text{ K}$  (room temperature). The (10, 10) SWCNTs are selected to be reinforcements in CNTRC, and the detailed material properties for different temperatures are listed in Table 1 [47]. The mass density of SWCNTs is taken to be  $1400 \text{ kg/m}^3$ . In computation, three volume fractions of CNTs (0.12, 0.17 and 0.28) are considered and the corresponding efficiency parameters are  $\eta_1 = 0.137$ ,  $\eta_2 = 1.022$  and  $\eta_3 = 0.715$  for

the case of  $V_{CN}^* = 0.12$ , and  $\eta_1 = 0.142$ ,  $\eta_2 = 1.626$  and  $\eta_3 = 1.138$  for the case of  $V_{CN}^* = 0.17$ , and  $\eta_1 = 0.141$ ,  $\eta_2 = 1.585$  and  $\eta_3 = 1.109$  for the case of  $V_{CN}^* = 0.28$ . For FRC, the volume fraction of graphite fibers is 0.6 and the material properties of which are [48]:  $E_{11}^f = 233.05 \text{ GPa}$ ,  $E_{22}^f = 23.1 \text{ GPa}$ ,  $G_{12}^f = 8.96 \text{ GPa}$ ,  $\nu^f = 0.2$ ,  $\alpha_{11}^f = -0.54 \times 10^{-6} \text{ K}^{-1}$ ,  $\alpha_{22}^f = 10.08 \times 10^{-6} \text{ K}^{-1}$  and  $\rho^f = 1750 \text{ kg/m}^3$ . The foundation is made of hydrogenated nitrile butadiene rubber (HNBR) filled with 21% carbon black (CB). The temperature-dependent properties of HNBR/CB [49] are  $\nu_s = 0.499$  and  $E_s = (29.6 - 0.25\Delta T + 0.0009\Delta T^2) \text{ MPa}$ . The above values are used in the following examples. In addition, we assume that out-plane shear moduli  $G_{13} = G_{12}$  and  $G_{23} = 1.2G_{12}$ . Two layups of hybrid laminated plate ( $[0^C/90^F]_2$  and  $[0^C/90^F]_s$ ) where the  $0^C$ -plies (i.e., CNTRC 0-plies) have different distributions of CNTs are considered. For the type 1, referred to as FG-1, the  $0^C$ -plies above the middle plane are FG-V types, while the  $0^C$ -plies below the middle plane are FG- $\Lambda$  types, whereas for the type 2, referred to as FG-2, the  $0^C$ -plies above the mid-plane are FG- $\Lambda$  types, while the  $0^C$ -plies below the mid-plane are FG-V types. It is assumed that the layers with the same layup angle contain the same matrix density. Then, the matrix crack density is expressed by  $(\rho_{crk}^0, \rho_{crk}^{90})$ , in which the superscripts 0 and 90 denote 0-plies and 90-plies, respectively. It is worth noting that the stiffness reduction model presented in Sect. 2 is adopted to UD-CNTRC layer, but not to FG-CNTRC layer.

#### 5.1 Validation

To validate the present method, four test examples for free and forced vibration of composite laminated plates and CNTRC plates are resolved.

The dimensionless natural frequencies of UD and FG-V CNTRC plates are calculated and compared in Table 2 with the finite element method (FEM) results

**Table 1** Temperature-dependent material properties for (10, 10) SWCNT [47]

$T$ (K)	$E_{11}^{CN}$ (TPa)	$E_{22}^{CN}$ (TPa)	$G_{12}^{CN}$ (TPa)	$\alpha_{11}^{CN} (\times 10^{-6}/\text{K})$	$\alpha_{22}^{CN} (\times 10^{-6}/\text{K})$
300	5.6466	7.0800	1.9445	3.4584	5.1682
400	5.5679	6.9814	1.9703	4.1496	5.0905
500	5.5308	6.9348	1.9643	4.5361	5.0189

**Table 2** Comparison of the dimensionless fundamental frequency ( $\bar{\omega} = \Omega_L(a^2/h)\sqrt{\rho_0/E_0}$ ) of CNTRC plates with simply supported boundary condition ( $a/b = 1, T = 300$  K)

$V_{CN}^*$	$b/h$	UD		FG-V	
		Zhu et al. [50]	Present	Zhu et al. [50]	Present
0.11	10	13.532	13.591	12.452	12.493
	20	17.355	17.339	15.110	15.093
	50	19.223	19.161	16.252	16.205
0.14	10	14.306	14.396	13.256	13.320
	20	18.921	18.940	16.510	16.519
	50	21.354	21.325	17.995	17.975
0.17	10	16.815	16.882	15.461	15.497
	20	21.456	21.430	18.638	18.611
	50	23.697	23.614	19.982	19.924

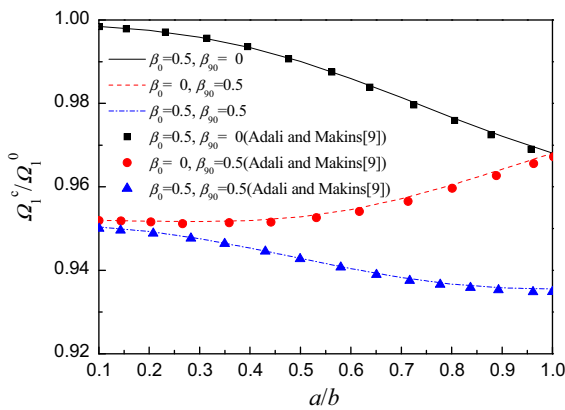


**Fig. 2** Comparisons of cracked to intact linear frequency ratios  $\Omega_1^c/\Omega_1^0$  for [0/90/0/90] laminated plates with various values of  $a/b$

of Zhu et al. [50] based on the first-order shear deformation plate theory. The dimensionless frequency is defined as  $\bar{\omega} = \Omega_L(a^2/h)\sqrt{\rho_0/E_0}$ , where  $\rho_0$  and  $E_0$  are the reference values of mass density and Young’s modulus of the matrix at room temperature. In this example, the CNT volume fractions and corresponding efficiency parameters  $\eta_j$  ( $j = 1, 2, 3$ ) are taken to be:  $\eta_1 = 0.149, \eta_2 = 0.934$  and  $\eta_3 = 0.934$  for the case of  $V_{CN}^* = 0.11$ , and  $\eta_1 = 0.150, \eta_2 = 0.941$  and  $\eta_3 = 0.941$  for the case of  $V_{CN}^* = 0.14$ , and  $\eta_1 = 0.149, \eta_2 = 1.381$  and  $\eta_3 = 1.381$  for the case of  $V_{CN}^*=0.17$ . Note that, in this example,  $G_{12} = G_{13} = G_{23}$ .

Secondly, the curves of linear fundamental frequency ratios ( $\bar{\omega} = \Omega_L(a^2/h)\sqrt{\rho_0/E_0}$ ) for matrix

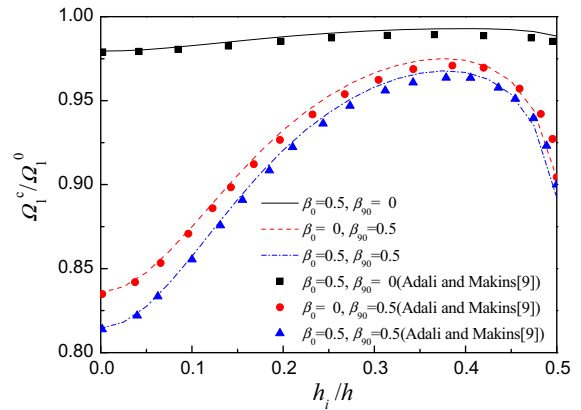


**Fig. 3** Comparisons of cracked to intact linear frequency ratios  $\Omega_1^c/\Omega_1^0$  for [0/90/0/90] laminated plates with various values of  $h_i/h$

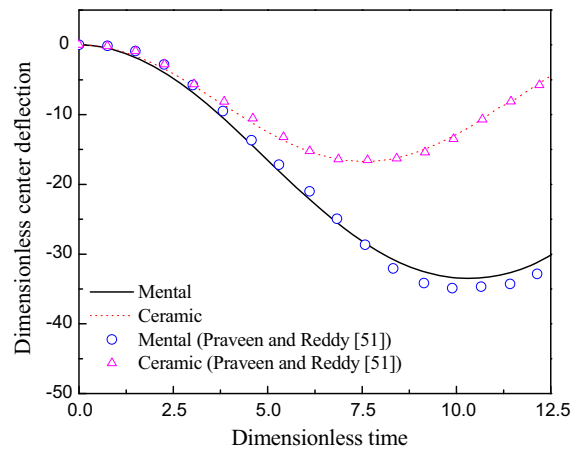


**Fig. 4** Comparisons of dynamic response for isotropic square plate subjected to a suddenly applied uniform load

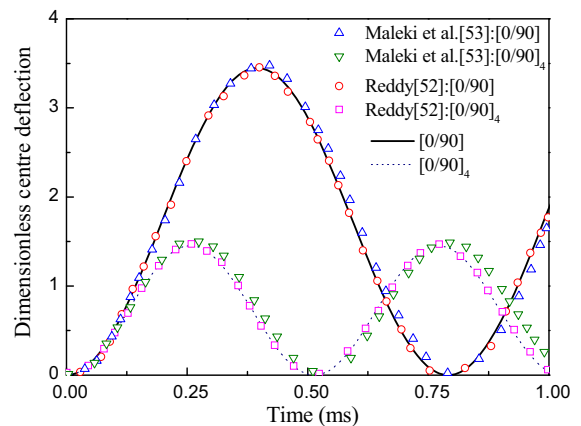


**Fig. 5** Comparisons of dynamic response for laminated plates subjected to a suddenly applied uniform load

**Table 3** Fundamental frequencies  $\tilde{\Omega} = \Omega_L(b^2/h)\sqrt{E_0/\rho_0}$  for  $[0^C/90^F]_2$  hybrid laminated plates with different values of  $b/h$  ( $a/b = 1$ ,  $T = 300$  K)

$V_{cn}^*$	$(\rho_{crk}^0, \rho_{crk}^{90})$		$b/h$					
			5	10	20	50	100	
0.12	(0, 0)	UD	11.1041	14.8861	16.7109	17.3677	17.4686	
		FG-1	11.4152	15.5087	17.5246	18.2564	18.3691	
		FG-2	10.6995	14.1757	15.8367	16.4329	16.5244	
	(0, 0.5)	UD	10.5103	14.2720	16.1210	16.7913	16.8945	
		FG-1	10.7711	14.8574	16.9366	17.7039	17.8228	
		FG-2	10.1502	13.5824	15.2331	15.8260	15.9171	
	(0.5, 0)	UD	10.8623	14.5960	16.4184	17.0794	17.1812	
		(0.5, 0.5)	UD	10.2626	13.9807	15.8280	16.5019	16.6059
0.17	(0, 0)	UD	12.1313	16.2484	18.2019	18.8970	19.0034	
		FG-1	12.4677	17.0112	19.2677	20.0902	20.2170	
		FG-2	11.6999	15.3719	17.0489	17.6352	17.7244	
	(0, 0.5)	UD	11.5450	15.6376	17.6368	18.3593	18.4704	
		FG-1	11.8274	16.3506	18.6984	19.5779	19.7149	
		FG-2	11.1675	14.7955	16.4735	17.0630	17.1528	
	(0.5, 0)	UD	11.7798	15.8288	17.7676	18.4609	18.5672	
		(0.5, 0.5)	UD	11.1853	15.2161	17.9214	17.9214	18.0322
0.28	(0, 0)	UD	12.7889	17.6812	20.2276	21.1827	21.3314	
		FG-1	13.1435	18.6083	21.6829	22.8952	23.0875	
		FG-2	12.4436	16.6588	18.6566	19.3672	19.4759	
	(0, 0.5)	UD	12.1398	16.9902	19.6548	20.6928	20.8567	
		FG-1	12.4346	17.8311	21.0777	22.4268	22.6452	
		FG-2	11.8780	16.0578	18.1028	18.8438	18.9579	
	(0.5, 0)	UD	12.4358	17.2756	19.8092	20.7610	20.9093	
		(0.5, 0.5)	UD	11.7759	16.5817	19.2358	20.2700	20.4334

cracking to intact matrix with different values of  $a/b$  and  $h_i/h$  are compared in Figs. 2 and 3 with the theoretical results of Adali and Makins [9] based on the classical laminated thin plate theory. In Figs. 2 and 3,  $h_i$  is defined as the thickness of inner layers (the second and third layers) of  $[0/90/0/90]$  plate. The plate is made of graphite/epoxy, and the material properties are:  $E_{11} = 132.4$  GPa,  $E_{22} = E_{33} = 10.8$  GPa,  $G_{12} = G_{13} = 5.65$  GPa,  $\nu_{12} = \nu_{13} = 0.24$  while  $\nu_{23} = 0.49$ .

As a comparison for dynamic response, the curves of central deflection as function of time for isotropic square plates subjected to a suddenly applied uniform load  $1.0 \times 10^6$  Pa are compared in Fig. 4 with the FEM results of Praveen and Reddy [51]. The side length and thickness of the plate are 0.2 m and 0.01 m, respectively. Two kinds of isotropic materials are considered. The

material properties are  $E = 70$  GPa,  $\nu = 0.3$  and  $\rho = 2707\text{kg/m}^3$  for aluminum, and  $E = 151$  GPa,  $\nu = 0.3$  and  $\rho = 3000\text{kg/m}^3$  for zirconia. The dimensionless deflection is defined as  $\bar{W} E_m h / q_0 a^2$ , while dimensionless time is defined as  $t \sqrt{E_m / (a^2 \rho)}$ . Note that the effect of temperature field is not considered in this example.

Finally, the curves of central deflection as function of time for a laminated plate subjected to a suddenly applied uniform load are plotted and compared in Fig. 5 with the analytical results of Reddy [52] and the generalized differential quadrature (GDQ) method results of Maleki et al. [53]. Both the length and width of the plate are 25 cm, and the thickness is 1 cm. Each ply is idealized as a homogeneous orthotropic material and is also assumed to have the same thickness. The mass density of the plate is  $8 \times 10^{-6}$  Ns<sup>2</sup>/cm<sup>4</sup>, and mechan-

**Table 4** Fundamental frequencies  $\tilde{\Omega} = \Omega_L(b^2/h)\sqrt{E_0/\rho_0}$  for  $[0^C/90^F]_s$  hybrid laminated plates with different values of  $b/h$  ( $a/b = 1$ ,  $T = 300$  K)

$V_{cn}^*$	$(\rho_{crk}^0, \rho_{crk}^{90})$		$b/h$					
			5	10	20	50	100	
0.12	(0, 0)	UD	11.2865	14.9450	16.7103	17.3459	17.4435	
		FG-1	11.6898	15.7915	17.8821	18.6573	18.7775	
		FG-2	10.7781	13.9721	15.4227	15.9291	16.0061	
	(0, 0.5)	UD	9.82282	13.7304	16.1301	17.1343	17.2970	
		FG-1	10.0672	14.3700	17.1938	18.4297	18.6334	
		FG-2	9.49547	12.9685	14.9425	15.7291	15.8542	
	(0.5, 0)	UD	11.0229	14.5882	16.3048	16.9220	17.0167	
	(0.5, 0.5)	UD	9.55101	13.3767	15.7266	16.7084	16.8673	
	0.17	(0, 0)	UD	12.2062	16.8290	19.3603	20.3381	20.4919
			FG-1	12.6005	17.7583	20.7628	21.9678	22.1599
FG-2			11.7073	15.7524	17.8146	18.5796	18.6983	
(0, 0.5)		UD	10.6226	15.3419	18.6148	20.1044	20.3536	
		FG-1	10.8574	16.0213	19.8611	21.7043	22.0196	
		FG-2	10.3133	14.5311	17.2184	18.3707	18.5591	
(0.5, 0)		UD	11.8190	16.3224	18.7865	19.7369	19.8863	
(0.5, 0.5)		UD	10.2148	14.8347	18.0441	19.5017	19.7452	
0.28		(0, 0)	UD	12.8374	18.8312	22.8727	24.6600	24.9555
			FG-1	13.2166	19.8256	24.5929	26.8102	27.1844
	FG-2		12.4179	17.7170	20.9915	22.3558	22.5763	
	(0, 0.5)	UD	11.0266	16.7548	21.6658	24.3248	24.8044	
		FG-1	11.2483	17.4318	23.1151	26.4063	27.0196	
		FG-2	10.8227	16.0318	20.0773	22.0878	22.4367	
	(0.5, 0)	UD	12.4601	18.3729	22.3639	24.1261	24.4172	
	(0.5, 0.5)	UD	10.6150	16.2848	21.1587	23.7907	24.2647	

ical properties are:  $E_{22} = 2.1 \times 10^{-6}$  N/cm<sup>2</sup>,  $E_{11} = 25E_{22}$ ,  $G_{12} = G_{13} = 0.5E_2$ ,  $G_{23} = 0.2E_{22}$  and  $\nu_{12} = 0.25$ . These four comparison studies show that the results from the present method are in good agreement with the existing results.

## 5.2 Free vibration

Several numerical examples are provided to investigate the free vibration of hybrid laminated plates with matrix cracking. Tables 3, 4, 5 and 6 show the effects of crack density on the fundamental frequencies of the  $[0^C/90^F]_2$  and  $[0^C/90^F]_s$  hybrid laminated plates under both movable and immovable end conditions at  $T = 300$ K, 400K and 500K. Two types (FG-1 and FG-2)

of FG-CNTRC layers are considered, and UD-CNTRC layers are also considered as a comparator. In the case of movable end conditions, the initial in-plane force is not considered here. Hence, the natural frequency of the plate with movable ends is the same as that of the same plate with immovable ends at  $T=300$  K, as shown in Tables 5 and 6. It can be seen that the natural frequencies are decreased with increase in crack density and temperature, but are increased with increase in CNT volume fraction. The different values of  $b/h$  are also considered in Tables 3 and 4. It can be seen that the natural frequencies rise with increase in  $b/h$ . From Table 5, it can be seen that the natural frequencies of the unsymmetric cross-ply laminated plate with movable ends are different from those of the same plate with immovable ends when the temperature rise

**Table 5** Comparisons of fundamental frequencies  $\tilde{\Omega} = \Omega_L(b^2/h)\sqrt{E_0/\rho_0}$  for  $[0^C/90^F]_2$  hybrid laminated plates with different values of  $b/h$  ( $a/b = 1, b/h = 20, T = 400$  and  $500$  K)

$V_{cn}^*$	$(\rho_{crk}^0, \rho_{crk}^{90})$		Immovable end conditions		Movable end conditions		
			$T = 400$ K	$T = 500$ K	$T = 400$ K	$T = 500$ K	
0.12	(0, 0)	UD	16.4132	16.1280	16.4375	16.1508	
		FG-1	17.2174	16.9229	17.2402	16.9442	
		FG-2	15.5451	15.2644	15.5710	15.2890	
	(0, 0.5)	UD	15.8920	15.6626	15.9017	15.6707	
		FG-1	16.6919	16.4455	16.7003	16.4524	
		FG-2	15.0166	14.7996	15.0276	14.8089	
	(0.5, 0)	UD	16.1563	15.8995	16.1767	15.9211	
		(0.5, 0.5)	UD	15.6207	15.4241	15.6406	15.4409
0.17	(0, 0)	UD	17.8757	17.5615	17.8944	17.5784	
		FG-1	18.9242	18.5910	18.9410	18.6061	
		FG-2	16.7349	16.4321	16.7550	16.4506	
	(0, 0.5)	UD	17.3828	17.1140	17.3769	17.1089	
		FG-1	18.4188	18.1217	18.4120	18.1159	
		FG-2	16.2411	15.9934	16.2349	15.9882	
	(0.5, 0)	UD	17.4874	17.2207	17.5091	17.2420	
		(0.5, 0.5)	UD	16.9809	16.7635	16.9908	16.7721
	0.28	(0, 0)	UD	19.8656	19.5109	19.8804	19.5239
			FG-1	21.2836	20.8839	21.2951	20.8939
			FG-2	18.3258	18.0049	18.3412	18.0187
(0, 0.5)		UD	19.3525	19.0253	19.3416	19.0161	
		FG-1	20.7270	20.3426	20.7141	20.3317	
		FG-2	17.8463	17.5673	17.8329	17.5560	
(0.5, 0)		UD	19.4864	19.1795	19.5096	19.2007	
		(0.5, 0.5)	UD	18.9647	18.6879	18.9703	18.6926

is under consideration. In contrast, from Table 6, for the symmetric cross-ply laminated plate, the thermal bending moments vanish and the results for the symmetric cross-ply laminated plate with either movable or immovable end conditions are identical. It can be seen that the unsymmetric cross-ply laminated plate with movable ends has a higher natural frequency than the same plate with immovable ends does at  $T = 400$  and  $500$  K. It can also be seen that the natural frequency of the hybrid laminated plate with FG-1  $0^C$ -plies is higher than that of the hybrid laminated plate with UD  $0^C$ -plies, whereas the hybrid laminated plate with FG-2  $0^C$ -plies is lower than that of the hybrid laminated plate with UD  $0^C$ -plies.

Table 7 presents the nonlinear-to-linear frequency ratios  $\omega_{NL}/\omega_L$  for  $[0^C/90^F]_2$  and  $[0^C/90^F]_s$  hybrid

laminated square plates at  $T = 300$  K,  $400$  and  $500$  K. The dimensionless frequency is defined as  $\tilde{\Omega} = \Omega_L(b^2/h)\sqrt{E_0/\rho_0}$ . The CNT volume fraction is taken to be  $0.12$ , and  $b/h$  is taken to be  $20$ . It can be seen that the fundamental frequencies are reduced, but the nonlinear-to-linear frequency ratios are increased with increase in temperature. The results show that the fundamental frequencies of FG-1 CNTRC plate are higher, but the nonlinear-to-linear frequency ratios of the same plate are lower than those of plates with uniform or unsymmetrical distribution of CNTs. Hence, in the following examples, except for Fig. 9, only FG-1-type hybrid laminated plate is considered. The plate end conditions are assumed to be immovable.

Figures 6, 7 and 8 show, respectively, the effects of crack density, CNT volume fraction and founda-

**Table 6** Comparisons of fundamental frequencies  $\tilde{\Omega} = \Omega_L(b^2/h)\sqrt{E_0/\rho_0}$  for  $[0^C/90^F]_s$  hybrid laminated plates with different values of  $b/h$  ( $a/b = 1$ ,  $b/h = 20$ ,  $T = 400$  and  $500$  K)

$V_{cn}^*$	$(\rho_{crk}^0, \rho_{crk}^{90})$		Immovable end conditions		Movable end conditions		
			$T = 400$ K	$T = 500$ K	$T = 400$ K	$T = 500$ K	
0.12	(0, 0)	UD	16.4327	16.1669	16.4327	16.1669	
		FG-1	17.5842	17.2966	17.5842	17.2966	
		FG-2	15.1623	14.9137	15.1623	14.9137	
	(0, 0.5)	UD	15.8280	15.5215	15.8280	15.5215	
		FG-1	16.8620	16.5210	16.8620	16.5210	
		FG-2	14.6671	14.3911	14.6671	14.3911	
	(0.5, 0)	UD	16.0802	15.8691	16.0802	15.8691	
		(0.5, 0.5)	UD	15.4778	15.2263	15.4778	15.2263
0.17	(0, 0)	UD	18.9980	18.6408	18.9980	18.6408	
		FG-1	20.3684	19.9748	20.3684	19.9748	
		FG-2	17.4789	17.1511	17.4789	17.1511	
	(0, 0.5)	UD	18.2119	17.7931	18.2119	17.7931	
		FG-1	19.4148	18.9445	19.4148	18.9445	
		FG-2	16.8542	16.4813	16.8542	16.4813	
	(0.5, 0)	UD	18.4991	18.2194	18.4991	18.2194	
		(0.5, 0.5)	UD	17.7162	17.3749	17.7162	17.3749
0.28	(0, 0)	UD	22.4042	21.9208	22.4042	21.9208	
		FG-1	24.0638	23.5095	24.0638	23.5095	
		FG-2	20.5752	20.1535	20.5752	20.1535	
	(0, 0.5)	UD	21.1278	20.5460	21.1278	20.5460	
		FG-1	22.5037	21.8349	22.5037	21.8349	
		FG-2	19.6077	19.1088	19.6077	19.1088	
	(0.5, 0)	UD	21.9620	21.5476	21.9620	21.5476	
		(0.5, 0.5)	UD	20.6870	20.1737	20.6870	20.1737

tion stiffness on the nonlinear-to-linear frequency ratios  $\omega_{NL}/\omega_L$  of  $[0^C/90^F]_s$  hybrid laminated plates. The plate geometric parameter  $a/b = 1$  and  $b/h = 20$ . In Fig. 6, the CNT volume fraction is taken to be 0.12, and the temperature is  $T = 300$  K. Three crack densities are considered. The crack densities are  $(\rho_{crk}^0, \rho_{crk}^{90}) = (0.5, 0.0)$  for the case of the cracks occurring only in CNTRC 0-ply,  $(\rho_{crk}^0, \rho_{crk}^{90}) = (0.0, 0.5)$  for the case of the cracks occurring only in FRC 90-ply,  $(\rho_{crk}^0, \rho_{crk}^{90}) = (0.5, 0.5)$  for the case of the cracks occurring in both CNTRC 0-ply and FRC 90-ply and  $(\rho_{crk}^0, \rho_{crk}^{90}) = (0.0, 0.0)$  for the plate without any matrix cracks. It can be found that the nonlinear-to-linear frequency ratio curves become lower when the cracks occur. For UD-type  $[0^C/90^F]_s$  laminated plate, the nonlinear-to-linear frequency ratio curves for the

two cases of cracks occurring in 0-ply only and in 90-ply only are close. In Fig. 7, the CNT volume fraction is taken to be 0.12, 0.17 and 0.28, and in Fig. 8, the CNT volume fraction is taken to be 0.28. In Figs. 7 and 8, the temperature is taken  $T = 400$  K, and the crack densities are taken to be (0.5, 0.5) for the UD-type CNTRC and (0.0, 0.5) for the FG-1-type CNTRC. Note that in Fig. 8 TD represents the material properties of foundation that are temperature dependent and TID represents the material properties of foundation that are independent of temperature, i.e.,  $E_s = 29.6$  MPa. The depth of the foundation is taken  $H_s = 20$  mm, whereas  $H_s = 0$  means the plate without any elastic foundation. Like in the case of intact laminated plate, the nonlinear-to-linear frequency ratio curves are decreased with increase in CNT volume fraction or

**Table 7** Comparisons of nonlinear-to-linear ratios  $\omega_{NL}/\omega_L$  for  $[0^C/90^F]_S$  hybrid laminated plates in thermal environments ( $a/b = 1$ ,  $b/h = 20$ ,  $V_{cn}^* = 0.12$ )

$(\rho_{crk}^0, \rho_{crk}^{90})$	$T$ (K)		$\tilde{\Omega}$	$\bar{W}_{max}/h$				
				0.2	0.4	0.6	0.8	1.0
(0, 0)	300	UD	16.7103	1.0407	1.1543	1.3222	1.5264	1.7545
		FG-1	17.8821	1.0357	1.1360	1.2859	1.4703	1.6778
		FG-2	15.4227	1.0477	1.1792	1.3705	1.6005	1.8547
	400	UD	16.4327	1.0416	1.1573	1.3279	1.5353	1.7665
		FG-1	17.5842	1.0364	1.1386	1.2911	1.4783	1.6889
		FG-2	15.1623	1.0486	1.1826	1.3773	1.6107	1.8685
	500	UD	16.1669	1.0425	1.1605	1.3343	1.5451	1.7797
		FG-1	17.2966	1.0372	1.1415	1.2968	1.4873	1.7011
		FG-2	14.9137	1.0497	1.1864	1.3846	1.6218	1.8834
(0, 0.5)	300	UD	16.1301	1.0424	1.1604	1.3341	1.5447	1.7793
		FG-1	17.1938	1.0374	1.1424	1.2986	1.4901	1.7049
		FG-2	14.9425	1.0493	1.1849	1.3816	1.6172	1.8773
	400	UD	15.8280	1.0436	1.1646	1.3423	1.5573	1.7963
		FG-1	16.8620	1.0385	1.1463	1.3063	1.5020	1.7212
		FG-2	14.6671	1.0506	1.1895	1.3905	1.6309	1.8956
	500	UD	15.5215	1.0450	1.1695	1.3518	1.5720	1.8170
		FG-1	16.5210	1.0398	1.1509	1.3155	1.5161	1.7405
		FG-2	14.3911	1.0521	1.1949	1.4009	1.6466	1.9167
(0.5, 0)	300	UD	16.3048	1.0421	1.1592	1.3317	1.5411	1.7744
	400	UD	16.0802	1.0428	1.1617	1.3365	1.5485	1.7844
	500	UD	15.8691	1.0435	1.1644	1.3418	1.5566	1.7953
(0.5, 0.5)	300	UD	15.7266	1.0439	1.1656	1.3442	1.5603	1.8005
	400	UD	15.4778	1.0449	1.1693	1.3515	1.5714	1.8154
	500	UD	15.2263	1.0461	1.1737	1.3600	1.5844	1.8330

foundation stiffness. Moreover, when the foundations are TID, the nonlinear-to-linear frequency ratio curves fall further compared with the TD ones.

### 5.3 Forced vibration

For all cases below, the aspect ratio  $a/b$  of laminated plate is 1 and the width to thickness ratio  $b/h$  is 10. The deflected mode is taken to be  $(m, n) = (1, 1)$ . The time step for Runge–Kutta method is  $\Delta\tau = 0.5\mu s$ . The dynamic load is assumed to be a suddenly applied uniform load with  $q_0 = 1$  MPa. The boundary condition is assumed to be immovable ends. The layup of laminate is  $[0^C/90^F]_2$ .

Figure 9 presents the dynamic response of hybrid laminated plates with two types of FG-CNTRC layers.

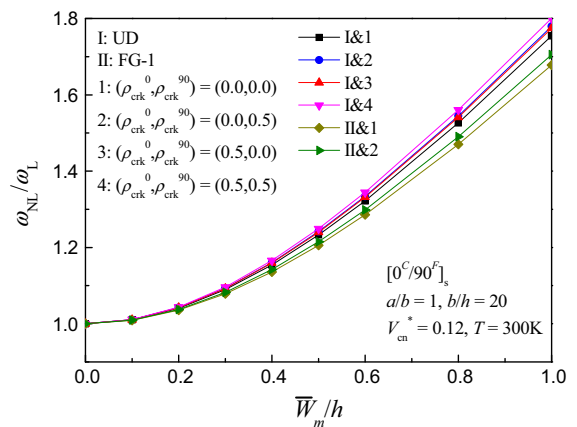


**Fig. 6** Effect of crack densities on the frequency–amplitude curves of hybrid laminated plates with doubly matrix cracking

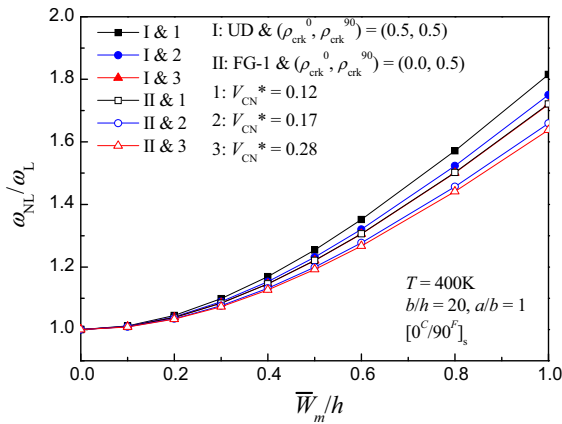


**Fig. 7** Effect of CNT volume fraction on the frequency–amplitude curves of hybrid laminated plates with doubly matrix cracking

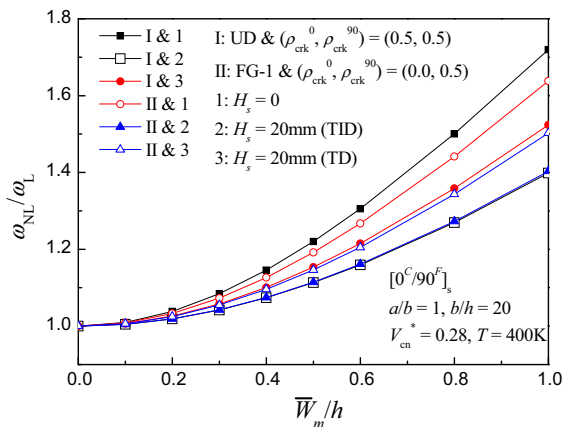


**Fig. 8** Effect of foundation stiffness on the frequency–amplitude curves of hybrid laminated plates with doubly matrix cracking

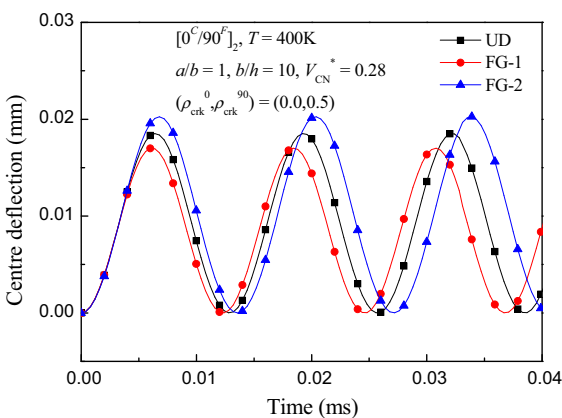


**Fig. 9** Effects of FG-CNTRC types on the dynamic response of matrix-cracked hybrid laminated plate

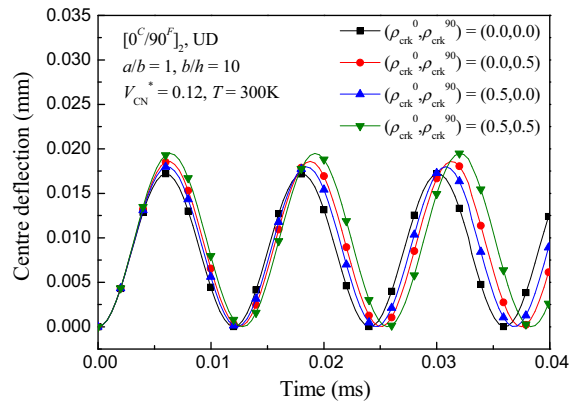


**Fig. 10** Effects of crack density on the dynamic response of matrix-cracked hybrid laminated plate

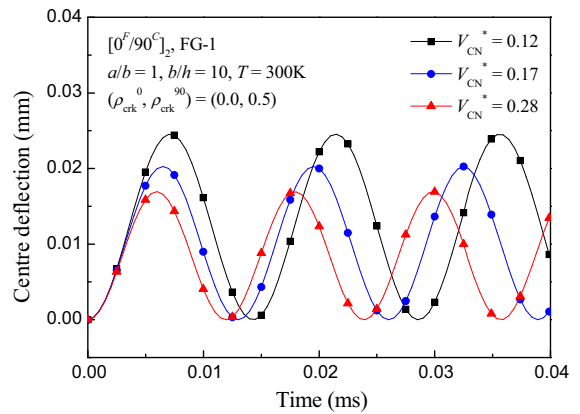
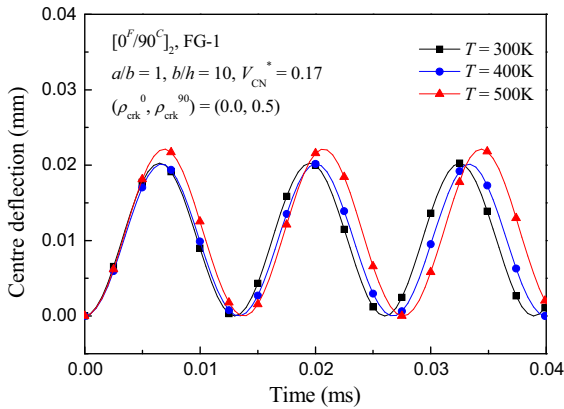


**Fig. 11** Effects of CNT volume fraction on the dynamic response of matrix-cracked hybrid laminated plate

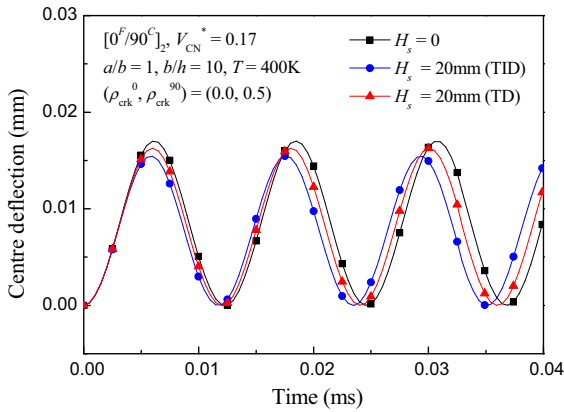
The results are also compared with those of the plate containing UD-CNTRC layers at  $T = 400\text{K}$ . The CNT volume fraction is taken to be 0.28, and the crack density for  $0^C$ -plies and  $90^F$ -plies is taken to be (0.0, 0.5). It can be found that the plate with FG-1-type CNTRC layer has the lowest central deflection, while the plate with FG-2-type CNTRC layer has the highest central deflection.

Figure 10 shows the effect of the crack density on the dynamic response of hybrid laminated plates with UD-CNTRC layers at room temperature ( $T = 300\text{K}$ ). The CNT volume fraction is taken to be 0.12. As expected, the central deflection is higher when the density of matrix cracks is increased. It is worth noting that the crack occurring in  $90$ -plies may have greater influence on the central deflection of the plate than the same crack occurring in  $0$ -plies.





**Fig. 12** Effects of temperature on the dynamic response of matrix-cracked hybrid laminated plate



**Fig. 13** Effects of foundation stiffness on the dynamic response of matrix-cracked hybrid laminated plate

Figures 11, 12 and 13 show, respectively, the effects of the CNT volume fraction, temperature change and foundation stiffness on the central deflection of  $[0^C/90^F]_2$  hybrid laminated plates with FG-1-type CNTRC layers. The crack densities are taken to be (0.0, 0.5). From Fig. 11, it can be seen that under the room temperature ( $T = 300$  K), the central deflection becomes lower when the CNT volume fraction is increased. In Fig. 12, the CNT volume fraction is taken to be 0.17. The results show that the central deflection becomes higher when temperature rises. In Fig. 13, we study the effect of foundation stiffness on the central deflection of the plate with  $V_{CN}^* = 0.17$  at  $T = 400$  K. The material properties are the same as used in Fig. 8. It can be found that the curve of central deflection versus time becomes lower when foundation stiffness is increased.

### 6 Conclusions

Nonlinear dynamic responses of matrix-cracked hybrid laminated plates resting on a Pasternak elastic foundation in thermal environments have been presented on the basis of a refined self-consistent model and a higher-order shear deformation plate theory. Two cases of in-plane boundary conditions are considered. The parametric studies have been carried out after four comparison studies which demonstrated the accuracy and effectiveness of the present method. The numerical results illustrate that the matrix crack has a significant effect on the linear frequencies and dynamic responses of hybrid laminated plates, but this effect is less pronounced on the nonlinear-to-linear frequency ratios of the same plate. The crack density also plays an important role on the dynamic deflections of the plate.

**Acknowledgments** The authors wish to thank Professor H.-S. Shen of Shanghai Jiao Tong University for his considerable support.

### Appendix

In Eqs. (47) and (48),

$$\begin{aligned} \Theta_1 &= \alpha_{311} - \alpha_{313} - \alpha_{331}, \\ g_{42} &= -\frac{4}{3\pi^2 mn} \gamma_{14} \gamma_{24} m^2 n^2 \beta^2 \left( \frac{\gamma_8}{\gamma_6} + \frac{\gamma_9}{\gamma_7} + 4 \frac{g_{05}}{g_{06}} \right) \\ &\quad \times (1 - \cos m\pi)(1 - \cos n\pi), \\ g_{43} &= -g_{41} \Theta_1, \\ g_4 &= -g_{08}^* - \gamma_{14} \gamma_{24} \frac{g_{05}^* g_{07}}{g_{06}} \\ &\quad - \left[ \gamma_{170} - \gamma_{171}(m^2 + n^2 \beta^2) \right] \\ &\quad - \gamma_{80} \left( \frac{m^2 g_{04} + n^2 \beta^2 g_{03}}{g_{00}} \right. \\ &\quad \left. - \gamma_{14} \gamma_{24} \frac{m^2 g_{02} + n^2 \beta^2 g_{01}}{g_{00}} \frac{g_{05}}{g_{06}} \right), \end{aligned}$$

for the case of immovable edge conditions

$$\begin{aligned} g_{41} &= Q_{11} + 2g_{42} \Phi(T), \\ \alpha_{311} &= -\frac{\gamma_{14} \gamma_{24}}{16 Q_{11}} \left[ \frac{m^4}{\gamma_7} + \frac{n^4 \beta^4}{\gamma_6} \right. \\ &\quad \left. + 2 \frac{m^4 + \gamma_{24}^2 n^4 \beta^4 + 2\gamma_5 m^2 n^2 \beta^2}{\gamma_{24}^2 - \gamma_5^2} \right], \\ \beta^2 B_{00}^{(0)} &= \gamma_{T1} \Delta T, b_{00}^{(0)} = \gamma_{T2} \Delta T, \end{aligned}$$

$$\begin{aligned}\beta^2 B_{00}^{(2)} &= -\frac{1}{8}\gamma_{24}\frac{m^2 + \gamma_5 n^2 \beta^2}{\gamma_{24}^2 - \gamma_5^2} \left(A_{11}^{(1)}\right)^2, b_{00}^{(2)} \\ &= -\frac{1}{8}\gamma_{24}\frac{\gamma_5 m^2 + \gamma_{24}^2 n^2 \beta^2}{\gamma_{24}^2 - \gamma_5^2} \left(A_{11}^{(1)}\right)^2,\end{aligned}$$

and for the case of movable edge conditions

$$\begin{aligned}g_{41} &= Q_{11}, \alpha_{311} \\ &= -\frac{\gamma_{14}\gamma_{24}}{16Q_{11}} \left[ \frac{m^4}{\gamma_7} + \frac{n^4\beta^4}{\gamma_6} \right], \beta^2 B_{00}^{(0)} = b_{00}^{(0)} = 0, \\ \beta^2 B_{00}^{(2)} &= b_{00}^{(2)} = 0,\end{aligned}$$

In the above equations (with others are defined as in [54]),

$$\begin{aligned}Q_{11} &= g_{08} + \gamma_{14}\gamma_{24}\frac{g_{05}g_{07}}{g_{06}} + \left[ K_1 + K_2 (m^2 + n^2\beta^2) \right], \\ Q_{13} &= g_{138} + \gamma_{14}\gamma_{24}\frac{g_{135}g_{137}}{g_{136}} + \left[ K_1 + K_2 (m^2 + 9n^2\beta^2) \right] \\ Q_{31} &= g_{318} + \gamma_{14}\gamma_{24}\frac{g_{315}g_{317}}{g_{316}} + \left[ K_1 + K_2 (9m^2 + n^2\beta^2) \right], \\ \alpha_{313} &= \frac{\gamma_{14}\gamma_{24}n^4\beta^4}{16Q_{13}\gamma_6}, \alpha_{331} = \frac{\gamma_{14}\gamma_{24}n^4\beta^4}{16Q_{31}\gamma_7}\end{aligned}$$

## References

- Irwin, G.R.: Analysis of stresses and strains near the end of a crack traversing a plate. *J. Appl. Mech.* **24**, 361–367 (1957)
- Krawczuk, M.: Natural vibrations of rectangular plates with a through crack. *Arch. Appl. Mech.* **63**, 491–504 (1993)
- Qu, G.M., Li, Y.Y., Cheng, L., Wang, B.: Vibration analysis of a piezoelectric composite plate with cracks. *Compos. Struct.* **72**, 111–118 (2006)
- Rzayev, O.G., Akbarov, S.D.: Natural vibrations of a composite plate strip with macrocracks. *Int. Appl. Mech.* **38**, 1281–1283 (2002)
- Chen, Y.C., Hwu, C.: Boundary element method for vibration analysis of two-dimensional anisotropic elastic solids containing holes, cracks or interfaces. *Eng. Anal. Bound. Elem.* **40**, 22–35 (2014)
- Massabò, R., Campi, F.: An efficient approach for multilayered beams and wide plates with imperfect interfaces and delaminations. *Compos. Struct.* **116**, 311–324 (2014)
- Moon, T.C., Kim, H.Y., Hwang, W.: Natural-frequency reduction model for matrix-dominated fatigue damage of composite laminates. *Compos. Struct.* **62**, 19–26 (2003)
- Umesh, K., Ganguli, R.: Shape and vibration control of a smart composite plate with matrix cracks. *Smart Mater. Struct.* **18**, 025002 (2009)
- Adali, S., Makins, R.K.: Effect of transverse matrix cracks on the frequencies of unsymmetrical, cross-ply laminates. *J. Frankl. Inst.* **329**, 655–665 (1992)
- Tong, J., Guild, F.J., Ogin, S.L., Smith, P.A.: On matrix crack growth in quasiisotropic laminates I. Experimental investigation. *Compos. Sci. Technol.* **57**, 1527–1535 (1997)
- Varna, J., Joffe, R., Akshantala, N.V., Talreja, R.: Damage in composite laminates with off-axis plies. *Compos. Sci. Technol.* **59**, 2139–2147 (1999)
- Shen, H.-S.: *A Two-step Perturbation Method in Nonlinear Analysis of Beams, Plates and Shells*. Wiley, Singapore (2013)
- Reddy, J.N.: A simple high-order shear deformation for laminated composite plate. *J. Appl. Mech.* **51**, 745–752 (1984)
- Nuismer, R.J., Tan, S.C.: Constitutive relations of a cracked composite lamina. *J. Comp. Mater.* **22**, 306–321 (1988)
- Henaff-Gardin, C., Lafarie-Frenot, M.C., Gamby, D.: Doubly periodic matrix cracking in composite laminates Part 1: general in-plane loading. *Compos. Struct.* **36**, 113–130 (1996)
- Henaff-Gardin, C., Lafarie-Frenot, M.C., Gamby, D.: Doubly periodic matrix cracking in composite laminates Part 2: thermal biaxial loading. *Compos. Struct.* **36**, 131–140 (1996)
- Renard, J.: Modelling of a damaged composite specimen by a micro-macro numerical simulation. In: *Proceedings of the 13th Annual ASME-ETCE Composite Materials Symposium*, pp. 57–62 (1990)
- Gudmundson, P., Ostlund, S.: First order analysis of stiffness reduction due to matrix cracking. *J. Compos. Mater.* **26**, 1009–1030 (1992)
- Gudmundson, P., Zang, W.L.: An analytic model for thermoelastic properties of composite laminates containing transverse matrix cracks. *Int. J. Solids Struct.* **30**, 3211–3231 (1993)
- Dvorak, G.J., Laws, N., Hejazi, M.: Analysis of progressive matrix cracking in composite laminates I. Thermoelastic properties of a ply with cracks. *J. Compos. Mater.* **19**, 216–234 (1985)
- Hashin, Z.: Analysis of cracked laminate: a variational approach. *Mech. Mater.* **4**, 121–136 (1985)
- Varna, J., Berglund, L.: Multiple transverse cracking and stiffness reduction in cross-ply laminates. *J. Compos. Technol. Res.* **13**, 97–106 (1991)
- Fan, J., Zhang, J.: In-situ damage evolution and micro/macro transition for laminated composites. *Compos. Sci. Technol.* **47**, 107–118 (1993)
- Kashtalyan, M., Soutis, C.: Predicting residual stiffness of cracked composite laminates subjected to multi-axial inplane loading. *J. Compos. Mater.* **47**, 2513–2524 (2013)
- Kashtalyan, M., Soutis, C.: Modelling off-axis ply matrix cracking in continuous fibre-reinforced polymer matrix composite laminates. *J. Mater. Sci.* **41**, 6789–6799 (2006)
- Bonnet, P., Sireude, D., Garnier, B., Chauvet, O.: Thermal properties and percolation in carbon nanotube-polymer composites. *J. Appl. Phys.* **91**, 201910 (2007)
- Liew, K.M., Lei, Z.X., Zhang, L.W.: Mechanical analysis of functionally graded carbon nanotube reinforced composites: a review. *Compos. Struct.* **120**, 90–97 (2015)
- Ajayan, P.M., Stephan, O., Colliex, C., Trauth, D.: Aligned carbon nanotube arrays formed by cutting a polymer resin-nanotube composite. *Science* **265**, 1212–1214 (1994)
- Thostenson, E.T., Chou, T.W.: Aligned multi-walled carbon nanotube-reinforced composites: processing and mechanical characterization. *J. Phys. D. Appl. Phys.* **35**, L77–L80 (2002)

30. Wang, Z.-X., Shen, H.-S.: Nonlinear vibration of nanotube-reinforced composite plates in thermal environments. *Comput. Mater. Sci.* **50**, 2319–2330 (2011)
31. Wang, Z.-X., Shen, H.-S.: Nonlinear dynamic response of nanotube-reinforced composite plates resting on elastic foundations in thermal environments. *Nonlinear Dyn.* **70**, 735–754 (2012)
32. Wang, Z.-X., Xu, J., Qiao, P.: Nonlinear low-velocity impact analysis of temperature-dependent nanotube-reinforced composite plates. *Compos. Struct.* **108**, 423–34 (2014)
33. Ansari, R., Hasrati, E., Faghieh Shojaei, M., Gholami, R., Shahabodini, A.: Forced vibration analysis of functionally graded carbon nanotube-reinforced composite plates using a numerical strategy. *Phys. E* **69**, 294–305 (2015)
34. Zhang, L.W., Lei, Z.X., Liew, K.M.: Free vibration analysis of functionally graded carbon nanotube reinforced composite triangular plates using the FSDT and element-free IMLS-Ritz method. *Compos. Struct.* **120**, 189–199 (2015)
35. Fan, Y., Wang, H.: Nonlinear vibration of matrix cracked laminated beams containing carbon nanotube reinforced composite layers in thermal environments. *Compos. Struct.* **124**, 35–43 (2015)
36. Laws, N., Dvorak, G.J., Hejazi, M.: Stiffness changes in Unidirectional composites caused by cracked systems. *Mech. Mater.* **2**, 123–137 (1983)
37. Shen, H.-S.: A comparison of buckling and postbuckling behavior of FGM plates with piezoelectric fiber reinforced composite actuators. *Compos. Struct.* **91**, 375–384 (2009)
38. Shen, H.-S.: Nonlinear bending of functionally graded carbon nanotube-reinforced composite plates in thermal environments. *Compos. Struct.* **91**, 9–19 (2009)
39. Shen, H.-S.: A novel technique for nonlinear analysis of beams on two-parameter elastic foundations. *Int. J. Struct. Stab. Dyn.* **11**, 999–1014 (2011)
40. Shapery, R.A.: Thermal expansion coefficients of composite materials based on energy principles. *J. Compos. Mater.* **2**, 380–404 (1968)
41. Shen, H.-S.: Nonlocal plate model for nonlinear analysis of thin films on elastic foundations in thermal environments. *Compos. Struct.* **93**, 1143–1152 (2011)
42. Shen, H.-S.: Kármán-type equations for a higher-order shear deformation plate theory and its use in the thermal postbuckling analysis. *Appl. Math. Mech.* **18**, 1137–1152 (1997)
43. Bhimaraddi, A.: Nonlinear free vibration of laminated composite plates. *J. Eng. Mech.* **118**, 174–189 (1992)
44. Singh, V.K., Panda, S.K.: Nonlinear free vibration analysis of single/doubly curved composite shallow shell panels. *Thin Wall. Struct.* **85**, 341–349 (2014)
45. Panda, S.K., Singh, B.N.: Non-linear free vibration analysis of laminated composite cylindrical/hyperboloidal shell panels based on higher order shear deformation theory using nonlinear finite-element method. *Proc. Inst. Mech. Eng. Part G. J. Aerosp. Eng.* **222**, 993–1006 (2008)
46. Pearson, C.E.: *Numerical Methods in Engineering and Science*. Van Nostrand Reinhold Company Inc., New York (1986)
47. Shen, H.-S., Zhang, C.-L.: Thermal buckling and post-buckling behavior of functionally graded carbon nanotube-reinforced composite plates. *Mater. Des.* **31**, 3403–3411 (2010)
48. Bowles, D.E., Tompkins, S.S.: Prediction of coefficients of thermal expansion for unidirectional composite. *J. Sound Vib.* **47**, 509–514 (1989)
49. Qu, M., Deng, F., Kalkhoran, S.M., Gouldstone, A., Robison, A., Van Vliet, K.J.: Nanoscale visualization and multi-scale mechanical implications of bound rubber interphases in rubber-carbon black nanocomposites. *Soft Matter* **7**, 1066–1077 (2011)
50. Zhu, P., Lei, Z.X., Liew, K.M.: Static and free vibration analyses of carbon nanotube-reinforced composite plates using finite element method with first order shear deformation plate theory. *Compos. Struct.* **94**, 1450–1460 (2012)
51. Praveen, G.N., Reddy, J.N.: Nonlinear transient thermoelastic analysis of functionally graded ceramic-metal plates. *Int. J. Solids Struct.* **35**, 4457–4476 (1998)
52. Reddy, J.N.: *Mechanics of Laminated Composite Plates and Shells Theory and Analysis*. CRC Press, London (2004)
53. Maleki, S., Tahani, M., Andakshideh, A.: Transient response of laminated plates with arbitrary laminations and boundary conditions under general dynamic loadings. *Arch. Appl. Mech.* **82**, 615–630 (2012)
54. Shen, H.-S.: Nonlinear bending response of functionally graded plates subjected to transverse loads and in thermal environments. *Int. J. Mech. Sci.* **44**, 561–584 (2002)